12-2009

Study of Take-Up Velocity in Enhancing Tensile Properties of Aligned Electrospun Nylon 6 Fibers

Johnny F. Najem
University of Akron Main Campus

STUDY OF TAKE-UP VELOCITY IN ENHANCING TENSILE PROPERTIES OF ALIGNED ELECTROSPUN NYLON 6 FIBERS

A Thesis

Presented to

The Graduate Faculty of The University of Akron

In Partial Fulfillment

of the Requirements for the Degree

Master of Science

Johnny F. Najem

December, 2009

STUDY OF TAKE-UP VELOCITY IN ENHANCING TENSILE PROPERTIES OF ALIGNED ELECTROSPUN NYLON 6 FIBERS

Johnny F. Najem

Thesis

Approved:	Accepted:
_____	_____
Advisor Dr. Shing-Chung Wong	Department Chair Dr. Celal Batur
_____	_____
Committee Member Dr. Sadhan C. Jana	Dean of the College Dr. George K. Haritos
_____	_____
Committee Member Dr. Zhenhai Xia	Dean of the Graduate School Dr. George R. Newkome
	_____
	Date

ABSTRACT

The variation of both the tensile properties and thermal properties of aligned electrospun fibers with the take-up velocity (TUV) of disc collector has not been widely investigated due to the difficulty of handling aligned nanofibers and measuring low loads. In this thesis, 25% of nylon 6 was dissolved in formic acid and then electrospun into fibers and the fibers were aligned using a rotating disc collector. We evaluated the tensile and thermal properties, average fiber diameter, crystallinity, crystalline morphology, molecular and crystalline orientation of aligned electrospun nylon 6 nanofibers as a function of TUV based on a disc collector. It was determined that by increasing the TUV from 14.2 m/s to 21.4 m/s, the tensile modulus and strength increased by 32% and 19% respectively while the elongation at break decreased by 44%. At the same time, the percentage of crystallinity, molecular and crystalline orientation increased by 21%, 11%, and 6% respectively while the average fiber diameter decreased by 40%. Meanwhile, the melting temperature and glass transition temperature of the fibers remained constant with increase of TUV.

ACKNOWLEDGEMENTS

First and foremost, I would like to thank my advisor Dr. Shing-Chung Wong for all his guidance, friendship, support, constant availability and willingness to answer my questions during the course of this study.

I would like to thank my committee members, Dr. Sadhan Jana and Dr. Zhenhai Xia, for their support and valuable help. I would also like to thank the Department of Mechanical Engineering, College of Polymer Engineering and Polymer Science at The University of Akron. I am deeply thankful to Dr. Avinash Baji and Dr. Reneker's group for helping me with electrospinning. I am also genuinely thankful for Dr. Stephen Z. D. Cheng for allowing me to use his X-ray machine and his student Mr. Xin Fei for helping me with the X-ray analysis.

I would like to thank all my friends including each member of Dr. Wong's group for their help and friendship.

Lastly, I would like to profoundly thank my father, Fares, mother, Rose, brothers Maroun and Elie, sister Marie-Therese, uncle Tony Owen, aunt Josephine, Chuck Owen and his family for all their support throughout my years of study at the university. I love all of you.

TABLE OF CONTENTS

Page

LIST OF TABLES

LIST OF FIGURES

CHAPTER I

INTRODUCTION

1.1. Overview on Electrospun Fibers

Nanomaterials can possess different mechanical properties from those of the bulk samples. This phenomenon might be happening as a result of the structure of the material or the geometrical confinement [1-12]. For electrospun fibers with a typical fiber diameter ranging from 20 to 1000 nm, the processing conditions have been shown to have an effect on the mechanical properties, the structures of the material, and the macromolecular conformation [1-5]. Applications for such nanofibers include reinforcing elements in composite materials, nanosensors, filter media, drug delivery carriers and tissue scaffolds. For several of these applications, the mechanical and the thermal properties are of utmost importance. Notable features of electrospinning are a high fiber elongation rate of about 1000/s and a reduction in the cross-sectional area of about one hundred thousands [1, 7]. Another attractable feature of the electrospinning process is the extremely quick formation of nanofibers, which is on a millisecond scale, and has been proven to promote the nucleation and the growth of polymer crystallites. These characteristics of electrospinning affect the orientation of the molecules within the nanofiber which is shown to have a direct impact on the mechanical properties of the nanofiber [3, 5, 8]. Inai et al. [9] studied the tensile properties of electrospun poly-L-lactide (PLLA) fibers. The tensile strength of these nanofibers was very close to the one

of the melt spun PLLA fibers while the elastic modulus of the nanofibers was lower than the one of the melt-spun fibers. Also, higher modulus and strength were obtained with an increasing TUV. For melt spun nylon 6 fibers, Gianchandani [13] and Bankar [14] determined that the tensile modulus and strength increased with the TUV while the elongation at break decreases. Gianchandani and Bankar also determined that the crystalline and amorphous orientations increased with the TUV for the melt spun fibers. For aligned electrospun fibers, Jose et al. [16] and Kongkhlang et al. [18] determined that the Herman's orientation function increases with increasing the TUV. Therefore, they concluded that the orientation of the crystalline phase in the fiber increases with the TUV while they also showed that the melting temperature was not affected. Furthermore, Jose et al. demonstrated, by electrospin-ning aligned nylon 6 nanofibers, that the percentage of α-form crystals increases with the TUV on the expense of γ-form crystals. That is noteworthy because the α-form crystals are known to have higher tensile modulus then the γ-form crystals [17].

1.2. Goals of Research

This research aims to study the variation of both tensile and thermal properties of aligned electrospun nylon 6 nanofibers with the TUV of a rotating disc collector. The study also addresses the effect of the TUV on average fiber diameter, crystalline and amorphous orientation, degree of crystallinity and crystalline morphology. Through this work, the nanotechnology field would profit from gaining more knowledge about the techniques used to test nanofibers and the obtained results.

CHAPTER II

LITERATURE REVIEW

2.1. History of Nylon 6

Aliphatic polyamides, known as nylons, were one of the first semi-crystalline polymers to be synthesized. The definition of nylon as described by Du Pont is the following [19]:

> "A generic term for any long chain synthetic polymeric amide which has recurring amid groups as an integral part of the main polymer chain and which is capable of being formed into a filament in which the structural elements are oriented in the direction of the axis."

In 1938, Schaaf et al. [20] discovered the first flourishing approach to synthesize ny- lon 6 in a commercial way. Meanwhile, Du Pont's Carothers [21] submitted patents for the commercial nylon known as nylon 6,6. This type of nylon was first synthesized in 1935 from adipic acid and hexamethylenediamine. In 1938, the first product to be marketed in the United States (U. S.) from these materials was a nylon filament. The first commercial production of nylon 6 from ε-caprolactam began in Germany in 1940. Because of their unique combination of properties, nylon turned out to be a commercial success instantly. Stockings were the first main market for these polymers. The synthesis of nylons was simple and economical, and the processing of these materials was easy for the fact of being thermoplastics. A high melting point extended the valuable service temperature

compared to other synthetic materials, and good mechanical properties made them ideal for applications which had been formerly restricted to metals.

Aliphatic polyamides, especially nylon 6 and nylon 6,6 have been used for several years in a broad range of applications from engineering plastics to frequent consumer goods, such as ski boots and power tool housings. Nowadays, greater than 3.5 billion pounds of polyamides are being produced annually in the U.S., where nylon 6 and nylon 6,6 comprise of 90% of the market. Furthermore, nylon 6 is still the fiber of choice for the majority of applications such as carpets, ropes, fabrics, and tire reinforcements. Nylon 6 possesses a good combination of high tensile strength, flexibility, toughness, chemical resistance, and a low coefficient of friction. Subsequently, it has been a preferred material for the latter applications. These beneficial properties are mainly due to its high melting temperature (220˚C) and polycaprolactam's high crystallinity (30 to 40%). In the past several years, the synthesis of this famous material has become inexpensive and relatively problem-free, which has been leading for many potential applications of this polymer. Though, nylon 6 has limitations including moisture absorption and low glass transition temperature by being compared to other engineering plastics. These may not seem as serious problems compared to the benefits mentioned above, but absorption of moisture, sometimes up to 10% in pure nylon6, can sternly diminish the mechanical properties of this polymer. Furthermore, moisture plasticizes the matrix lowering the glass transition and heat distortion temperatures by as much as 40˚C and leading to noticeable dimensional changes in molded samples.

The structure of nylon 6 is made of amide groups separated from each other by a series of five methylene sequences. Flory [22] derived the structure of the amide bond

and the connecting methylene units which are shown in Figure 2.1. The amide group is fundamentally planar due the partial double bond characteristic of the C-N bond. This could be seen by having shorter bond length compared to an aliphatic CH2-N bond.

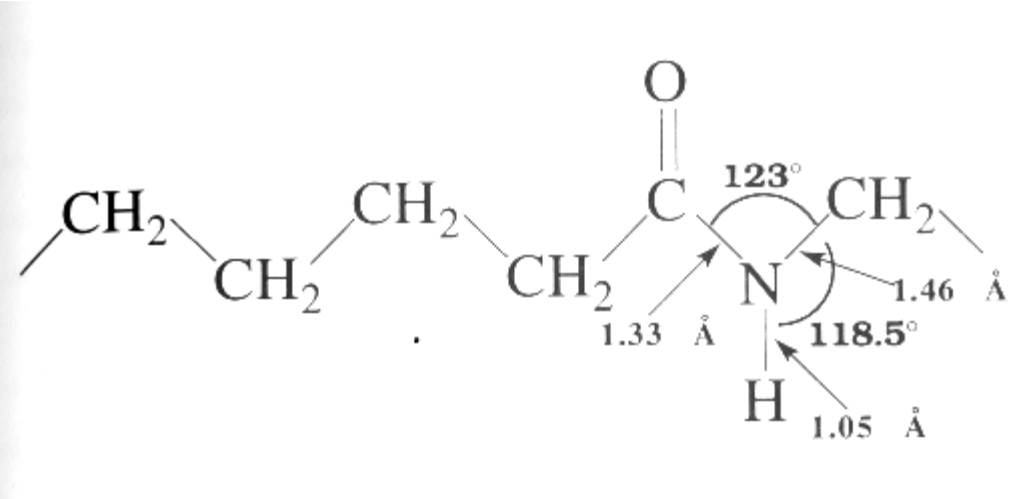

Figure 2.1 Schematic for repeat unit structure of nylon 6 including bond angles and bond lengths [22].

The unique properties seen for nylon 6 and other polyamides are present due mainly to the ability of the N-H bond groups on one chain to form strong hydrogen bonds with the C-O groups on a different chain. In addition, the mechanism of this hydrogen bonding plays an important role in determining the crystalline structure of nylon 6. These hydrogen bonds are intermolecular in nature and subsist in extended sheets in the nylon 6 crystals and in the amorphous regions.

2.1.1. Nylon 6 Synthesis

The ring-opening polymerization of lactams, specifically nylon 6, is a crucial method for the synthesis of several aliphatic polyamides. Although nylon 6 can be synthesized via polycondensation methods, the ring-opening polymerization generally results in higher molecular weights. Figure 2.2 shows a schematic of the initiation and propagation steps for three polymerization methods in the ring opening of nylon 6.

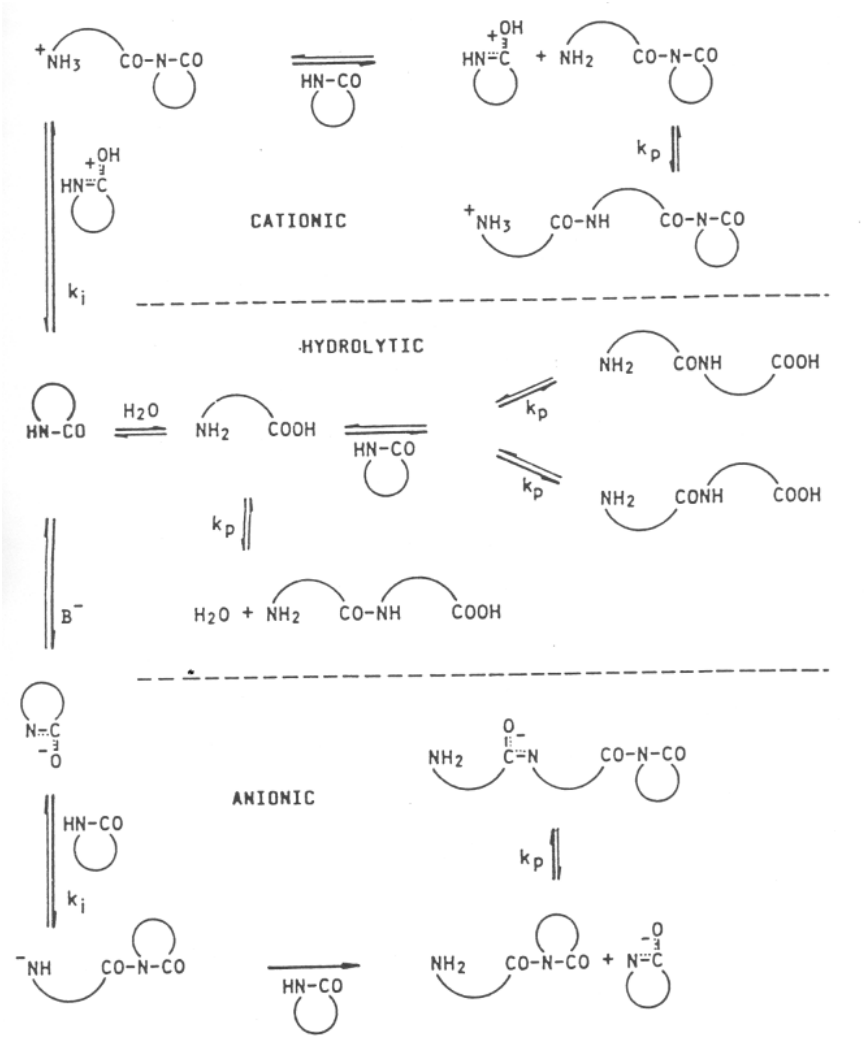

Figure 2.2 Schematic of initiation and propagation steps for the three polymerization methods in the ring-opening reaction of nylon 6 and other lactam polymers [23].

The ring-opening method of polymerizing nylon 6 consists of one general type of reaction, transamidation. ε – caprolactam is transamidized when the cyclic amide groups are converted to linear chains [23]. Figure 2.3 shows the step process for the synthesis of nylon 6 via the hydrolytic ring-opening polymerization of ε-caprolactam.

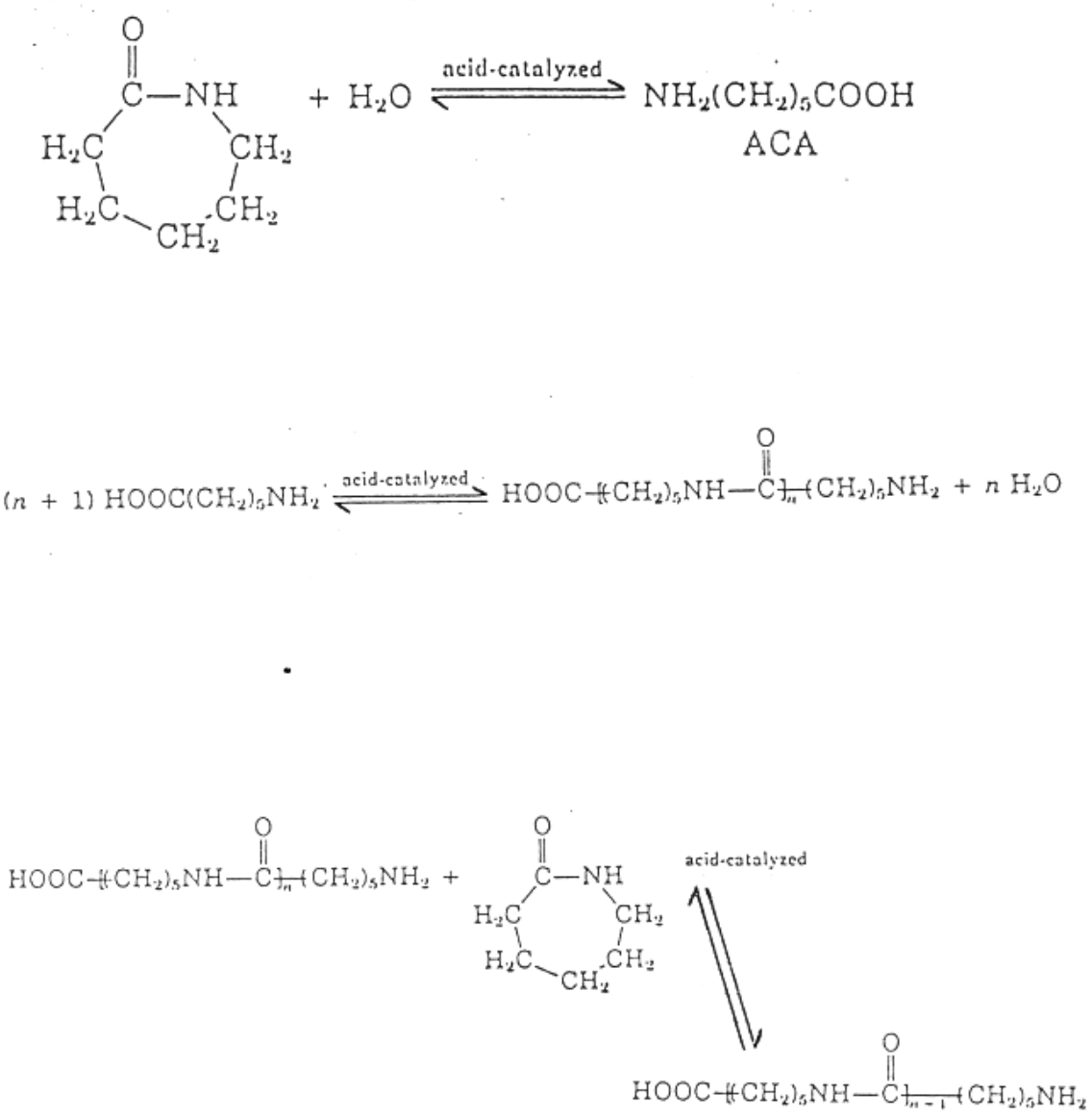

Figure 2.3 Schematic for synthesis of nylon 6 via the hydrolytic ring-opening polymerization of ε-caprolactam [24].

2.1.2 Thermodynamic Properties and Relaxation Behavior of Nylon 6

Nylon 6 has multifaceted thermodynamic and relaxation transitions which mainly originate from the hydrogen bonding characteristic of this polymer. The amide groups are polar and result in strong interchain attractions such as hydrogen bonding. This hydrogen bonding leads to finer values of toughness, rigidity and heat resistance compared with other engineering polymers. Due to the strong interchain interactions, a high degree of crystallinity can be achieved which leads to superior solvent resistance, tensile modulus and strength, and dimensional stability. Several researchers [25, 34] portrayed the thermal properties and relaxations of nylon 6.

Thermodynamically, the melting temperature (T_m) of a polymer is defined as the temperature of equilibrium coexistence of a polymer crystal with its melt [34].

Typically, T_m of nylon 6 is determined using differential scanning calorimetry (DSC). The T_m obtained from a DSC experiment depends on the polymer, experimental conditions and thermal history of the sample. Hence, it is necessary to give a range of melting temperatures rather than a specific temperature value. Depending on these factors and the crystalline structure of the nylon 6 lamellae, the melting temperature of nylon 6 is typically between 210 and 225˚C [25, 28-33].

The equilibrium heat of fusion, ΔH_f°, is a vital quantity and is necessary for the calculation of the degree of crystallinity. Researchers [25, 28-30] have found that ΔH_f° is 241 J/g for α-form crystals and 239 J/g for the γ- form crystals. Furthermore, the equilibrium melting temperature, T_m°, is an imperative thermodynamic property for nylon 6 among other polymers. It is defined as the melting temperature of infinitely large polymer crystals which enclose no defects. The value of T_m° has been determined to vary

from 250 to 260˚C for nylon 6 α-form crystals [25, 28-33] and from 230 to 235˚C for the γ-form crystals [30-33].

The glass transition temperature, T_g, of a polymer behaves like a second-order thermodynamic transition, but actually is not due to the kinetic dependence of this transition. The T_g is exclusively determined by the properties of the amorphous regions of the semi-crystalline polymer. The degree of crystallinity and the crystalline morphology affect the T_g, but only because they affect the mobility of the amorphous chains around the crystal structures. Moisture also has a significant effect on the glass transition of nylon 6. Knowing that several factors influence the glass transition temperature, such as the type of experiment and experimental conditions, it is essential to first list these particular parameters before giving specific values for the T_g. Using the DSC, researchers found that the T_g varies from 40 to 55˚C for dry samples [35-38]. When using dynamic mechanical experiments, the glass transition is determined to be between 55 and 65˚C [37-39]. Besides, the effect of the degree of crystallinity has been observed to increase the T_g by as high as 15˚C [37] while moisture and water decrease the T_g by 70˚C depending on the relative humidity (rh) [39].

For nylon 6 and other linear polyamides, there are usually several relaxation processes, including the glass transition. These relaxations have been studied experimentally using different methods including dynamic mechanical analysis (DMA), dielectric analysis (DEA), and nuclear magnetic resonnance (NMR) in both solution and solid state [40, 41]. These relaxations, viscoelastic in nature, depend on both frequency and temperature. The α-relaxation, which occurs at high temperature, is associated with the cooperative long range motion of the amorphous nylon 6 chains. Hence, this

relaxation is directly related to the glass transition of nylon 6 which could decrease by up to 70˚C with a large amount of moisture absorption [24].

β-relaxation is another relaxation process which takes place around -80˚C. This peak has been shown to be related to the presence of low molecular weight monomers or cyclic oligomers in the sample and to the absorption of moisture [42, 43]. This peak was nearly absent for dry samples and for samples not containing moisture nor low molecular weight (MW) compounds. The most credible molecular interpretation for this relaxation has to do with the kink motion of the amide groups which are not bound in a network of hydrogen bridges. Therefore, these groups move about the adjacent methylene units in the region of large free volume [24].

γ-relaxation is a third crucial secondary relaxation which arises around -130˚C. This energy absorption process is due to the kink motions of segments formed out of two or more CH2 groups in a high free volume region. It was determined that the intensity of the γ-relaxation peak increased with the number of CH2 groups [24, 44].

Plasticizers could affect the relaxation temperatures and molecular motion of nylon 6. These materials, such as moisture, are usually low molecular weight compounds added to decrease the glass transition temperature of a polymer by increasing the amount of free volume in the system. Monomer and low MW cyclic oligomers also plasticize nylon 6. Hence, they must be removed from the sample for maintaining a high T_g.

2.1.3. Crystal Structure and Morphology of Nylon 6

Nylon 6 could crystallize to a certain degree below 100%. WAXD and DSC are the most widespread methods employed to measure the degree of crystallinity. However,

the obtained degree of crystallinity from these different methods has been found to be significantly different [45- 51]. The glass transition is increased with crystallinity due to the constraint of mobility in the amorphous chains.

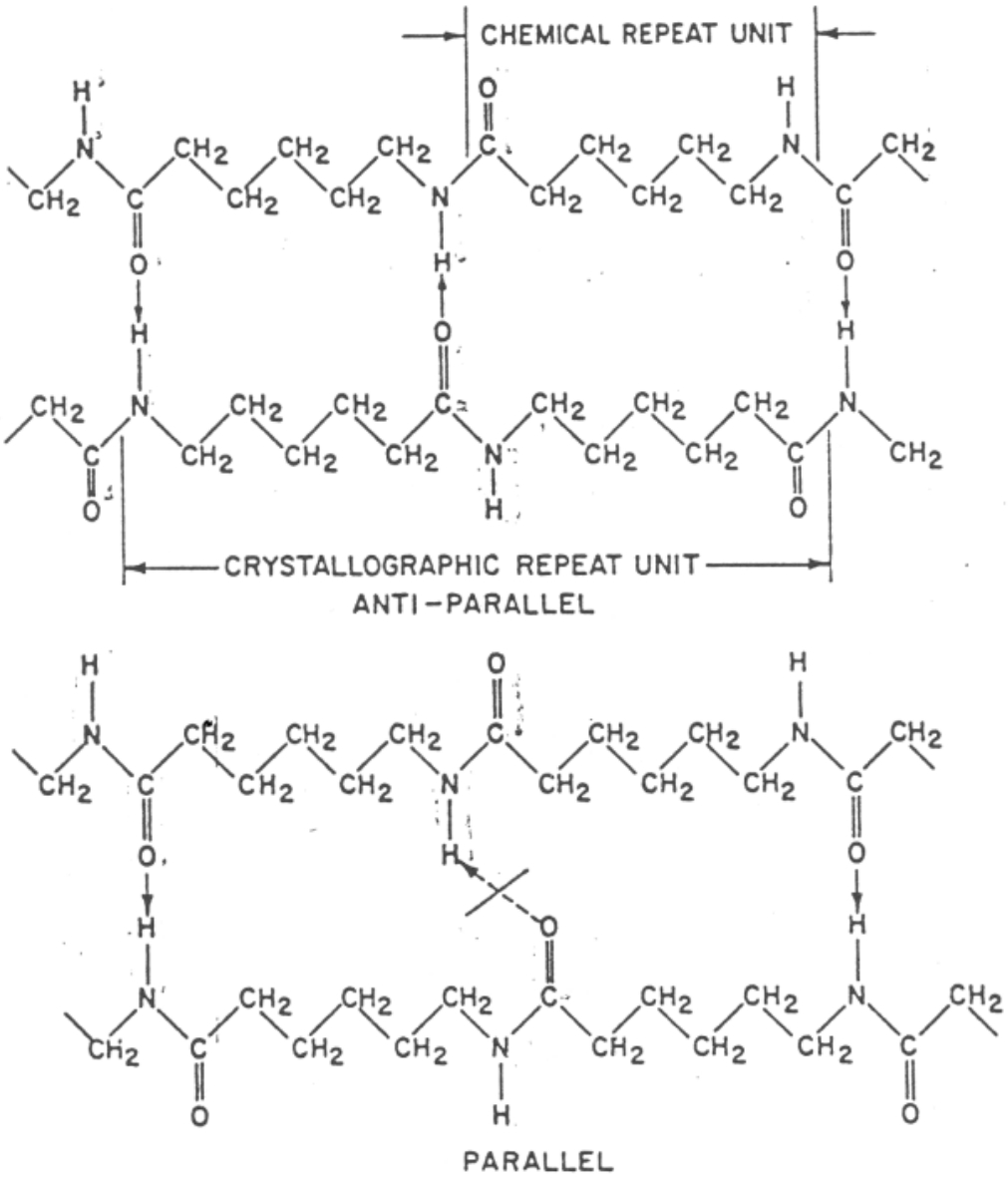

Figure 2.4 Schematic of parallel and anti-parallel orientations in hydrogen bonded sheets of nylon 6 crystals [52].

The lamellae play the role of physical crosslinks and reduce the cooperative motion of the interlamellar amorphous chains. Furthermore, the mechanical properties such as the tensile modulus and strength increase with the degree of crystallinity while toughness and impact strength decrease. Hydrogen bonding in the crystalline phase is complete and regular. Anti-parallel arrangement, shown in Figure 2.4, is the only achievable way for having complete hydrogen bonding in the crystallite sheets of extended planar chains [24].

The crystal structure is usually investigated using WAXD. The unit cell parameters and the orientations of the molecules can typically be found by using this method. Nylon 6 could simultaneously exist in different crystal structures, a phenomenon known as polymorphism. Hence, it is crucial to use this technique to characterize these crystal structures for determining the unit cell parameters for each structure.

Nylon 6 can crystallize into α-form crystals and γ-form crystals [52]. The α-form crystals can exist in which the hydrogen bonds are oriented between anti-parallel chains. Also, the γ-form crystal can exist in which the hydrogen bonds are oriented between parallel chains.

The α-form crystal has a monoclinic structure for which a = 0.956 nanometers (nm), the chain axis b = 1.724 nm, c = 0.801 nm, and the angle β = 67.5°. α -form crystals are characterized by two WAXD peaks which are located at about equatorial 2θ = 20°, known as 200 reflection, and 24°, known as 002/202 reflection. γ-form crystals have a monoclinic structure for which a = 0.933 nm, the chain axis b = 1.688 nm, c = 0.478 nm, and the angle β = 121°. γ-form crystals are characterized by two WAXD peaks which are located at about equatorial 2θ = 22°, known as 200 reflection, and 11°, known as 020 reflection [13, 26, 15, 27]. Figure 2.5 shows 2D WAXD scans for melt spun fibers.

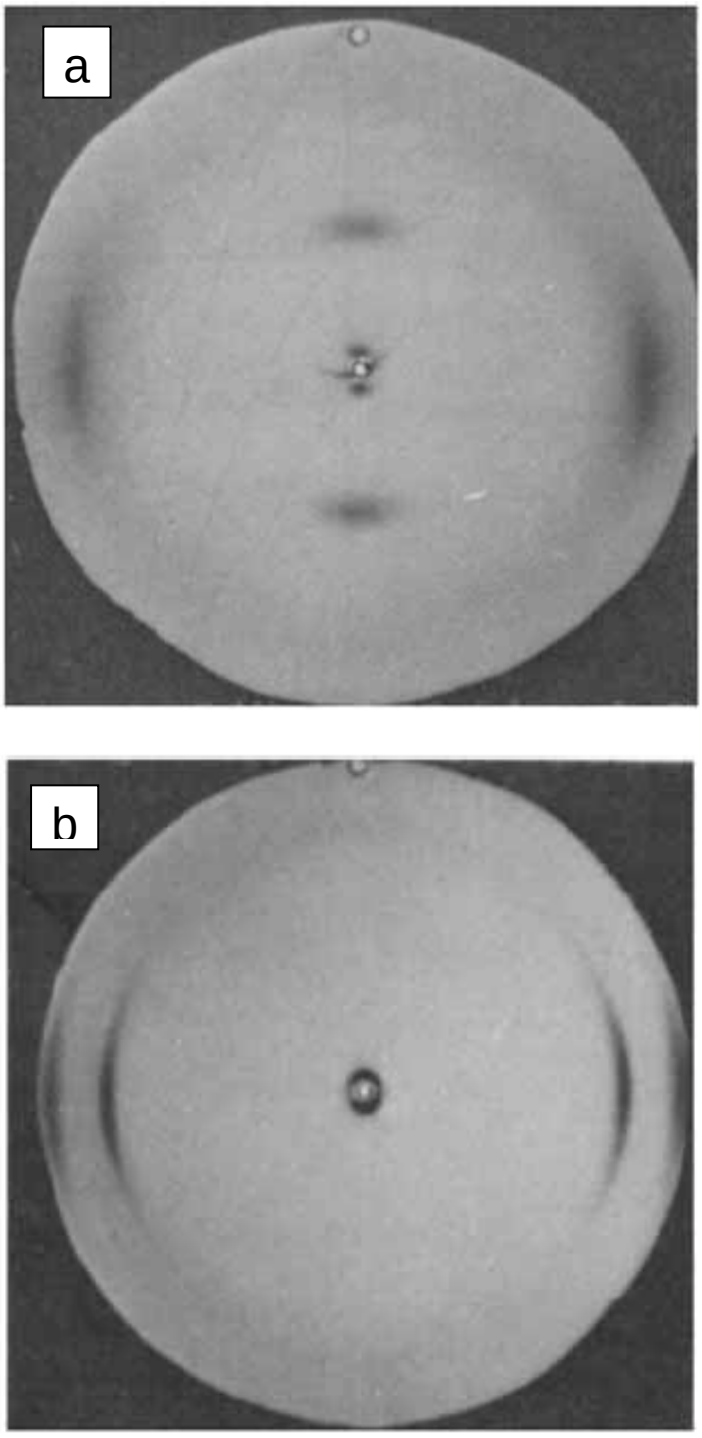

Figure 2.5 Representative 2D WAXD scans for melt spun nylon 6 fibers collected at a TUV of 1000m/min (a) immediately after spinning and (b) after annealing in formic acid at 120˚C for 2 hours [14].

Two main energies work together to decide which crystal structure of nylon 6 is stable at a particular set of experimental conditions. The first energy is connected to the twisting of the carbon-carbon double bond about its minimum energy conformation. The second energy is a function of the change in the direction or separation distance of the hydrogen bonds in nylon 6 [52]. Besides, stress along the polymer chain is expected to influence the crystal structure by restraining the twisting of the amide groups which is an essential occurrence for the existence of the γ-form crystals. In the γ-crystal, the balance of energies is primarily between the van der Waals interactions in the crystal lamellae and the twisting of the amide groups out of the plane. Hence, the hydrogen bonds always stay in their minimum energy conformation and enlarged methylene packing leads to a shortening of the unit cell chain axis because of this twist. Stress on the crystal from the neighboring amorphous areas could proscribe this twist. Subsequently, the driving force for α-form crystals formation becomes superior to that for the γ-form crystals [52].

The α- and γ-form crystals could be obtained depending on the ways of preparing the sample [53, 54]. Both forms with comparable compositions could be obtained by quenching a sample from the melt. From the other side, only the α-form crystal are found when the sample is annealed below the melting temperature or else crystallized with a low degree of supercooling, ($\Delta T = Tm^{\circ} - Tc$) <70 ˚C.

2.1.4. Physical and Mechanical Properties of Nylon 6

The physical and mechanical properties of nylon 6 could be affected by the molecular weight, crystal size, structure and degree of crystallinity. Plasticizing has a major effect on the mechanical and thermal properties of nylon 6. Moisture has a hefty

plasticizing effect on nylon 6: it increases the free volume and hence considerably decreases the glass transition or α-relaxation along with the tensile modulus and strength. The effect of plasticizer on the mechanical properties of nylon 6 is shown in Table 2.1.

The superior physical and tensile properties of nylon 6 offer this polymer several advantages over other thermoplastics. Nylon 6 has high tensile modulus and strength values, as a result of a fairly high crystallinity and strong intermolecular interactions. Furthermore, it possesses excellent low temperature toughness and impact strength properties. Also, this polymer has been appealing in industrial applications due to good chemical and environmental resistance along with superb dielectric properties.

Table 2.1 Effect of plasticizer on the mechanical properties of nylon 6. The amount of plasticizer increases from left to right [55].

Physical property	Standard	Flexible	More flexible	ASTM test method
tensile yield strength, MPa[a]	81	76	48	D638
flexural modulus, MPa[a]	2700	2415	1175	D790
notched Izod impact, J/m[b]				D256
at 23°C	58	80	106	
at −40°C	43		48	

[a] To convert MPa to psi, multiply by 145.
[b] To convert J/m to ftlbf/in., divide by 53.38.

In addition to the ones mentioned earlier, another drawback for nylon 6 is that the glass transition of a dry version of the polymer is relatively low at 50°C. Hence, the creep resistance is poor at temperatures much higher than room temperature.

The densities of α- and γ-form crystals are approximately 1.24 g/ cm^3 and 1.17 g/ cm^3, respectively [56]. Also, the density of the amorphous phase is 1.08 g/cm^3 [13]. Moisture has been found to have an insignificant effect on density [57]. Figure 2.6 shows

a schematic view of the moisture absorption while Table 2.2 shows the reported data on moisture absorption. For fibers or oriented films, moisture absorption exists [58- 60].

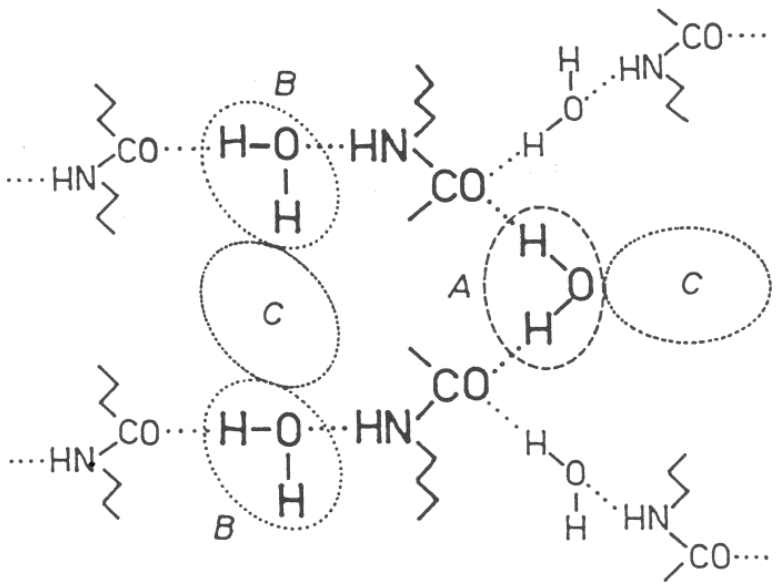

Figure 2.6 Schematic of water-amide complexes in linear polyamides used to explain the absorption of water [52].

The mechanical behavior of nylon 6 among other polymers depends considerably on their structures. Molecular, supramolecular, crystal, fibril, and macroscopic structure, including cracks are several structure stages which get involved in the relationship between structure and properties [24]. The tensile properties of nylon 6 have been widely studied in the past. The values reported for the tensile strength of dry (<0.5 % moisture content) nylon 6 samples vary between 60 to 80 MPa and the ones for tensile modulus fluctuate between 0.8 and 2.0 GPa [61, 62].

Table 2.2 Absorption of water by nylon 6 along with other nylons and the calculated and experimentally determined linear dimensional changes after the equilibrium absorption [119].

	Nylon-6 (Extracted)[a]	Nylon-610[a]	Nylon-12[b]
At 20°C, 65% R.H.:			
Reported % water absorbed	3.5-4.0	1.8-2.0	--
Reported % max. linear change	1.1-1.3	0.5-0.6	--
Calc'd linear change = (1/3) (% water)	1.2-1.3	0.6-0.7	--
At 20°C, 100% R.H.:			
Reported % water absorbed	8.5-10.0	3.2-3.8	1.4
Reported % max. linear change	2.8-3.0	0.9-1.2	0.2
Calc'd linear change = (1/3) (% water)	2.8-3.3	1.1-1.3	0.5

[a] Absorption and expansion data from Ref. 15.

[b] Expansion data from Ref. 45.

2.2. Melt Spinning Review

Melt spinning is a prominent method used for fibers production. Strain-induced crystallization can occur on the running threadline for spinning speeds greater than 3000 meters per minute (mpm) [63, 64]. Nylon 6 crystallizes on the bobbin, even though not usually crystallizing on the spin line, and the process speed is higher with increasing molecular orientation developed during spinning [65]. The orientation of the amorphous phase increases less sharply, but progressively increases in the range of a high draw ratios where the crystalline orientation no longer increased [66].

2.2.1. High Modulus Fibers

There has been emergent attention to the production of ultra high-modulus oriented polymers. It has been found, that in nylons and polyesters, there is an extensive gap between the initial moduli achieved and those anticipated from theoretical considerations. For nylon 6, commercial fibers have a tensile modulus of 4 GPa with comparison to theoretical value ranging between 165 and 300 GPa [67, 68, 69].

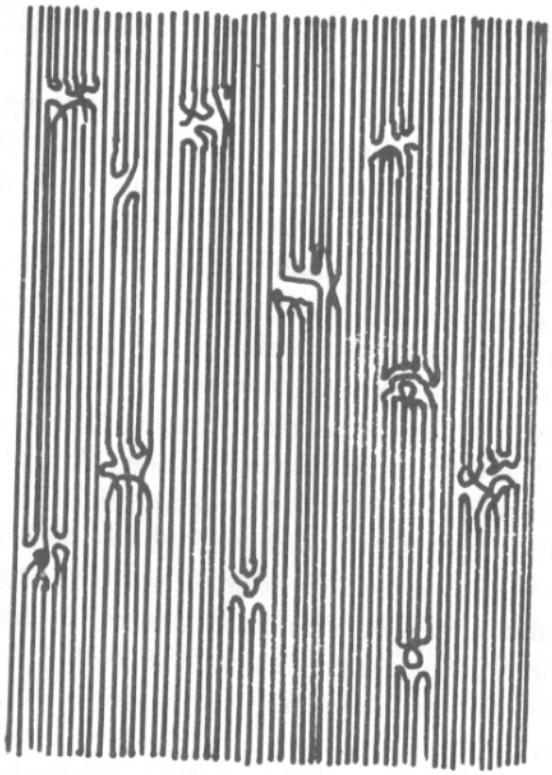

Figure 2.7 Schematic of continuous structure model of high modulus fibers.

A common way for obtaining high modulus fibers is changing the microfibrillar structure of customary fibers into continuous crystal structure, as shown in Figure 2.7 with little amount of randomly distributed structural distortions [70]. A transitional

between the microfibrillar and continuous structure models is the Prevorsek's "Swiss cheese" three phase model of highly drawn nylon 6 fibers shown in Figure 2.8 [71].

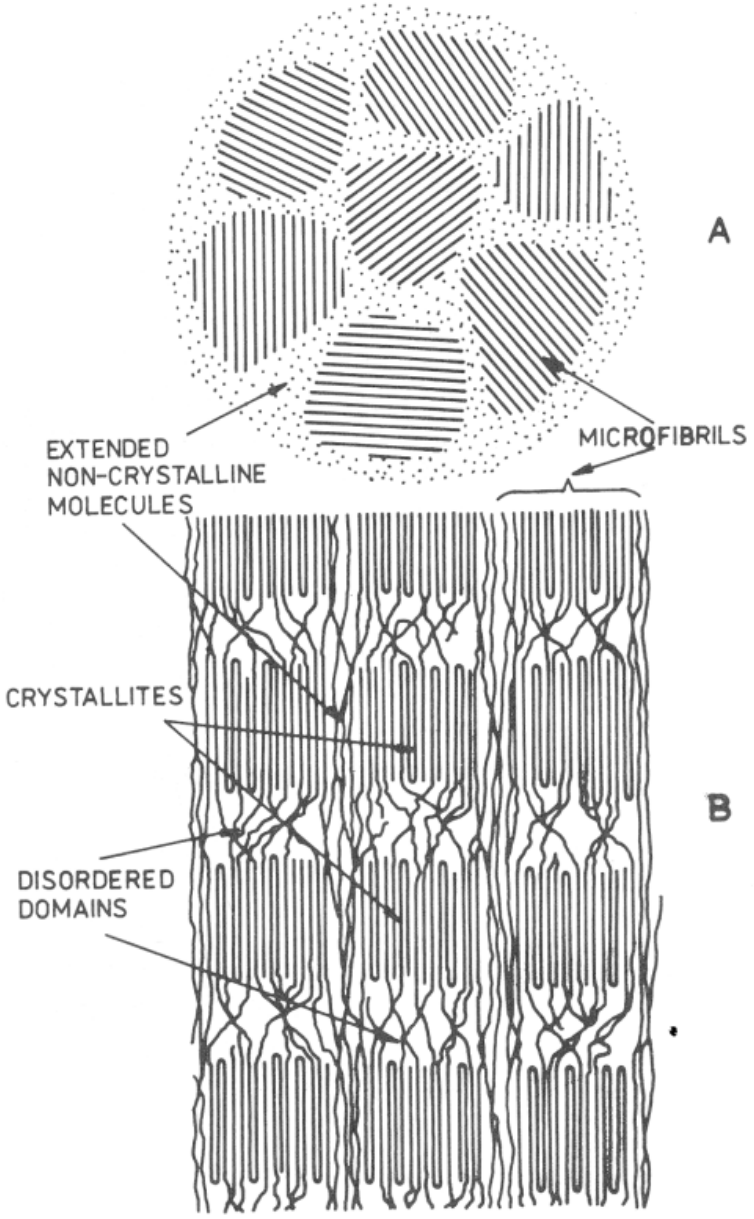

Figure 2.8 Schematic for structural model of nylon 6 fibers, (A) cross-sectional and (B) longitudinal views [71].

In order to obtain ultra high tenacity fibers, the following structural principles need to be satisfied: increasing the number of tie molecules and degree of molecular

orientation, decreasing the chain folding, and increasing the molecular length for dropping the intermolecular chain slip at polymer chain ends [70].

2.2.2. Yielding, Orientation, and Fibrillation

For unoriented crystalline polyamide, the crystalline lamellae are ordered in spherulites with more or less developed central symmetry. The boundaries of the spherulites are the weakest sites of the solid polymer and have a tendency to fail first in a mechanical testing [72]. Hence, they contribute to premature irrecoverable plastic deformation along with lamellar structure change and arrangement. Microscopic investigations and WAXD prove that, upon drawing, the semicrystalline polymers experience distinct structural changes. The initial lamellar or spherulitic morphology is changed into fibrillar structure with a stack of lamellae oriented along the draw direction.

It was determined that stretching the intercrystalline amorphous regions leads to the majority of the tensile deformation of nylon 6 fibers [73]. This deformation occurs at a mostly constant volume as interfibrillar amorphous material could liberally move within the microstructure.

2.2.3 High-modulus and High-strength Polyamide 6

The mechanical properties could be significantly increased through solid-state deformation as long as the exterior deformation leads to an efficient molecular chain orientation. Cold drawing, cold extrusion, and hydrostatic extrusion are three major processes used in the solid state deformation.

In the fiber industry, the cold drawing process involves stretching of spun fibers between two sets of rollers with the take-up roller rotating at a higher velocity than the feed roller [74]. Incremental drawing process is a substitute process for stretching in several successive steps. Continuous incremental drawing could be accomplished by drawing the fiber between two rotating cones. It has been shown that the latter process produces nylon 6 fibers with higher tensile modulus and strength and a higher degree of molecular orientation [74].

Although the theoretical strength must be about one-tenth of the tensile modulus [69], frequent polyamide fibers have a tensile strength of roughly 0.5 GPa [75-78]. In both crystalline and amorphous regions, hydrogen bonding obstructs the sliding of chains, thus preventing the increase in molecular orientation to a higher degree.

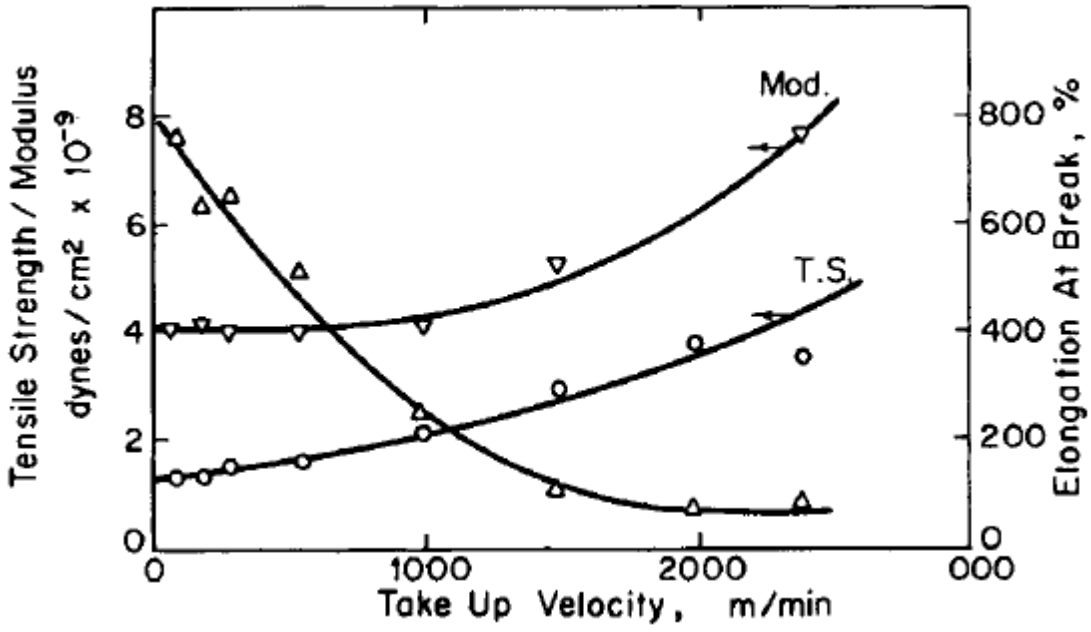

Figure 2.9 Plots of tensile modulus, tensile strength, and elongation at break vs. TUV [14].

However, fractional success in solving this issue has already been achieved by several procedures based on weakening the hydrogen bonds. The maximum DR in conventional nylon 6 drawing is about 5. Thus, using this method, higher draw ratio can be attained. One of the methods is plasticizing nylon 6 with liquid ammonia which is then removed after solid-state coextrusion [79]. Such plasticization only affects the amorphous phase [80]. Never-theless, the draw ratio increases and the tensile modulus increases to 13 GPa. For melt spun nylon 6 fibers, it has been determined that the tensile modulus and strength increase with the TUV while the elongation at break decreases [13, 14]. Figure 2.9 shows representative plots of the variation of the tensile modulus and strength and elongation at break with the TUV.

2.3. Electrospinning Process

Electrospinning is a method which uses electrostatic forces to produce fibers. It was first introduced by Formhals in 1934 [97] and more interest in this method has grown rapidly since the 1990's where Reneker [83, 84] has been making significant contributions. Electrospinning uses a high voltage source, in the range of 5 to 35 kilo volts (kV). During the process, the polymer solution becomes electrically charged and produces micro and nanofibers, with diameters ranging from a few nanometers and to greater than 5 μm [83]. Figure 2.10 illustrates the schematic of the electrospinning setup. Basically, the setup consists of a syringe or pipette partially filled with a polymer solution, a grounded conductive collecting plate and a high voltage source. The advantage of using the syringe equipped with a needle is having a more consistent size for the flow channel because the size of the needle is standard. A syringe pump is usually used for

controlling the solution's flow rate. The needle of the syringe serves as an electrode for electrically charging the solution.

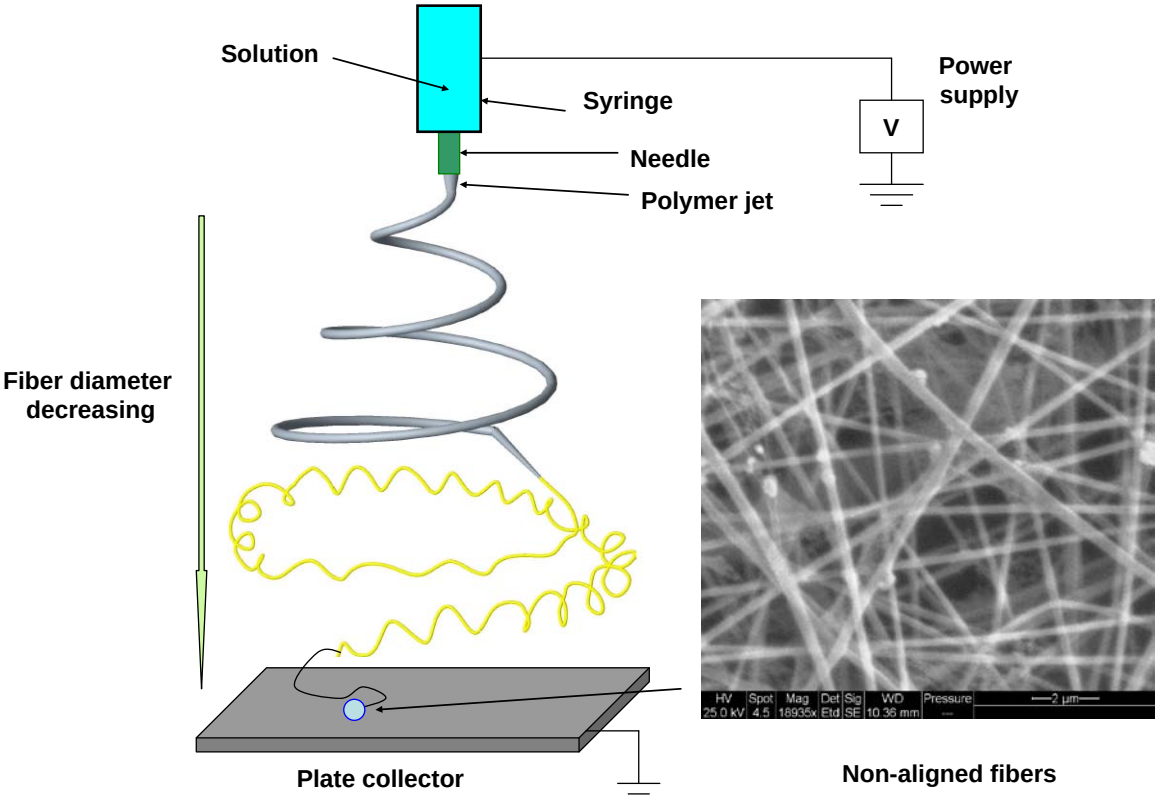

Figure 2.10 Schematic of electrospinning setup for collecting randomly oriented fibers.

Otherwise, the electrode could be engrossed into the solution. The needle-collector distance used in a laboratory setup is usually between 10 and 25 cm and the current ranges between a few hundred nanoamperes to a few microamperes. Because of the influence of a sturdy electrostatic field, charges are induced in the solution and charged polymer chains are accelerated towards the collector. If the strength of the electrostatic field is low, the pendant drop on the tip of the pipette is banned from dripping due to the solution's surface tension [98-100]. By increasing the intensity of the electric field, the

charges induced on the liquid surface fend off each other and hence generate shear stresses. These revolting forces act in the apposite direction of the surface tension [101], resulting in the pendant drop being extended into a conical shape which serves as an initiating surface [102-104]. Taylor derived the following expression for the critical voltage where the conical shape of the drop is preserved and equilibrium between forces exists:

$$V_c^2 = 4\left(\frac{H^2}{L^2}\right)\left(\ln\left(\frac{2L}{R}\right) - 1.5\right)(0.117\pi R\gamma) \qquad (1)$$

where V_c is the critical voltage , H distance between the collector and the tip of the pipette, L length of capillary tube, R radius of pipette, and γ surface tension of the solution.

2.3.1. Fiber Diameter Control

Several researchers investigated the effect of parameters on the diameter of fibers [105, 106]. The used electrospinning parameters have been shown to influence the morphology and diameter of the fibers. Key parameters controlling the diameter of the fiber are (1) type of used solvent, (2) flow rate of the solution, (3) concentration of polymer in the solution, and (4) conductivity of the solution. Mostly, surface tension, flow rate, and electric current of the solution control the diameter of the thrashing jet. For example, the fiber diameter was reduced 10 times by reducing the flow rate by 32 times or increasing the current carrying capacity of the jet by 32 times.

2.3.2. Fiber Alignment and Collection Methods

It was lately determined that the nature of the collector significantly influences the morphological and physical properties of spun fibers [107, 108]. The degree of charge

dissipation upon fiber deposition influences the density of the fibers per unit area on the collector and the fiber arrangement. Randomly oriented and aligned fibers could be formed using a stationary and rotating disc collector, respectively. The degree of anisotropy within an electrospun fibrous mat can greatly affect not only the mechanical properties but also cell adhesion, proliferation, and alignment. In several applications, it is desirable to develop an aligned fibrous mat [109-112]. For instance, it is enviable to generate aligned fibrous mats in designing scaffolds meant to replace highly oriented tissue such as the medial layer of a native artery. In the medial layer both smooth muscle cells and extracellular matrix ECM fibrils are aligned circumferentially allowing the vasoconstriction and vasodilatation in response to corresponding stimuli [113]. Several of the frequently used methods for aligning fibers are described below.

2.3.2.1. Rotating Drum Collector

This method is commonly used to collect aligned fibers. The diameter of the fiber could be controlled through the take-up velocity (TUV) of the drum [109-111].

The alignment of the fibers is induced by the rotating drum and the degree of fiber alignment improves with the rotational speed [109, 112]. Randomly oriented fibers are obtained on the drum at TUV lower than the fiber TUV. At higher TUV, the fibers extend before being collected on the drum due to a centrifugal force which is developed on the surface of the rotating drum [112, 114, 115]. However, much higher TUVs break the fiber and hence no more continuous fibers could be collected.

2.3.2.2 Rotating Disk Collector

This method is similar to the rotating drum collector and is used to obtain uniaxially aligned fibers. However, its advantage compared to the rotating drum collector is that most of the fibers are collected in an aligned fashion on the sharp-edged disk [114-117].

The jet travels in a conical and inverse conical path using the rotating disk collector compared to a conical path through using a drum collector. In its first stage, the jet follows the common envelope cone path caused by the instabilities manipulating the jet. The diameter of the loop decreases, at a position above the disk, as the conical shape of the jet starts to shrivel. Subsequently, an inverted cone appears with the tip of the cone resting on the disk. The applied electric field is concentrated on the sharp edge of the disk and therefore the polymer jet, being charged, is pulled towards the edge of the wheel. The fibers, being attracted to the edge of the disk, are collected on its perimeter because of the tangential force acting on the fibers. This force, generated from the rotation of the disk, stretches the fibers leading to a decreased of their diameters. A small quantity of aligned fibers is obtained due to the small area at the tip of the disk. Nevertheless, the alignment of the obtained fibers is of higher quality than the rotating drum.

2.3.2.3. Static Parallel Electrodes

The advantage of this method is that the setup is simple. Also, it is easy to collect single fibers and several aligned fibers for mechanical testing. A remaining electrostatic repulsion between the spun fibers is caused by the air gap between the electrodes assisting in the alignment of the fibers [85, 118-120]. Two nonconductive strips are

positioned along a straight line and an aluminum foil is placed on each of the strips and connected to the ground as shown in Figure 2.11. This technique facilitates the deposition of the aligned fibers.

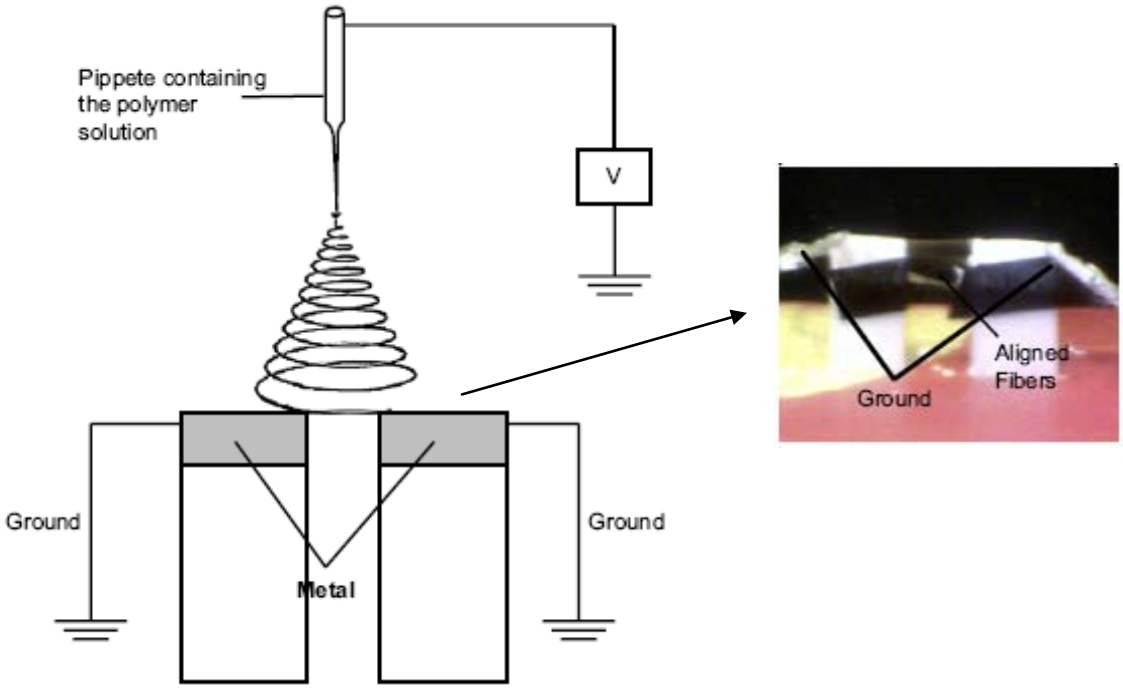

Figure 2.11 Schematic of static electrodes used for collecting aligned fiber bundles. The optical micrograph shows the aligned fibers collector using this technique.

2.3.3. Structural Properties of Electrospun Fibers

Electrospun fibers usually display structural hierarchy in most semi-crystalline polymers. While the fiber is being formed, a part of the chains crystallizes forming lamellae and the remaining polymer chains form the amorphous phase [121-123]. When shear and elongation forces are present, the lamellae organize in a fibril fashion. At the

same time, the tie chain molecules pass through the neighboring crystallites forming small sized bundles. The shear forces applied on the jet during electrospinning cause the orientation of the polymer chains along the fiber axis [121]. Konkhlang et al. [121] inspected the crystal morphology and molecular orientation of polyoxymethylene (POM) fiber. They concluded that each fiber consists of nanofibrils which are aligned and parallel to the fiber axis. The fibrils are made of 14 polymer chains and 40 monomeric units.

2.3.3.1 Molecular Orientation

The polymer jet, being influenced by the electrostatic field, experiences a high degree of elongation strain, about ten thousand times the draw ratio, and where the draw rate is over 106 s^{-1}. The shear forces and high elongation strains are capable of aligning the macromolecular chains along the fiber axis leading to a high degree of molecular orientations to the fibers [85-88, 123]. Zong et. al. [124] determined that the molecular chains in the electrospun PLLA fibers have high orientation compared to random-coil shape chains in the PLLA film. Transmission electron microscopy (TEM) could be used to analyze the chain orientation by staining the fibers with ink. There is a phase contrast between the amorphous and crystalline lamellae when the fibers are analyzed using the TEM. Table 2.3 shows the increase of this factor with TUV for electrospun nylon 6 nanofibers. The molecular orientation could also be determined using X-ray diffraction analysis.

Table 2.3 Variation of Herman's orientation factor with TUV for nylon 6 electrospun fibers [16].

Effect of take-up speed and MWNT on the orientation

Take-up speed (rpm)	Herman's orientation factor		
	Neat Nylon 6	Nylon 6/0.1 wt% MWNT	Nylon 6/1.0 wt% MWNT
3000	0.149	0.14	0.155
4500	0.172	0.23	0.18
6000	0.204	0.19	0.19

Furthermore, draw ratio can be used to have an estimate of the molecular orientation because it calculates the amount of extension the jet undergoes during electrospinning [85, 112, 125-127]. From the other side, for nylon 6 and polyoxymethylene electrospun fibers, Herman's orientation factor has been determined to increase with TUV [16, 18].

2.3.3.2. Crystallinity

The crystallinity in the fibers is thereby influenced by the rate of solvent evaporation [114, 128]. One of the most common techniques employed to measure the degree of crystallinity is wide angle X-ray diffraction (WAXD) analysis.

Lee et al. [129] and Reneker et al. [130] determined that the crystalline structure in fibers is developed in many polyester and ductile materials. They argue that crystallinity in the fiber can be higher than the unprocessed polymer pellets. They also claim that electrospinning inhibits the development of crystallinity specifically for rigid polymers with high T_g values. However, ductile polymers and polyesters with lower T_g values take longer period of time to crystallize. Hence, ductile polymers have the possibility of crystallization during the jet drawing and elongation process, even after the fibers are solidified. Other researchers also showed that the degree of crystallinity

increased with the TUV [18]. Besides, for 200 nm diameter electrospun nylon 6 fibers, it has been determined that the content of the α-form crystals increases with the TUV [16].

2.3.3.3. Effect of Fiber Diameter on the Structural Properties

Zussman et al. [131] show that the electrospun fibers acquire a skin-core morphology. The properties of the skin differ from the properties of the core. The skin layers are distinguished by oriented layered planes whereas the core of the fiber has randomly oriented chains. These results are authenticated by molecular dynamic simulation results.

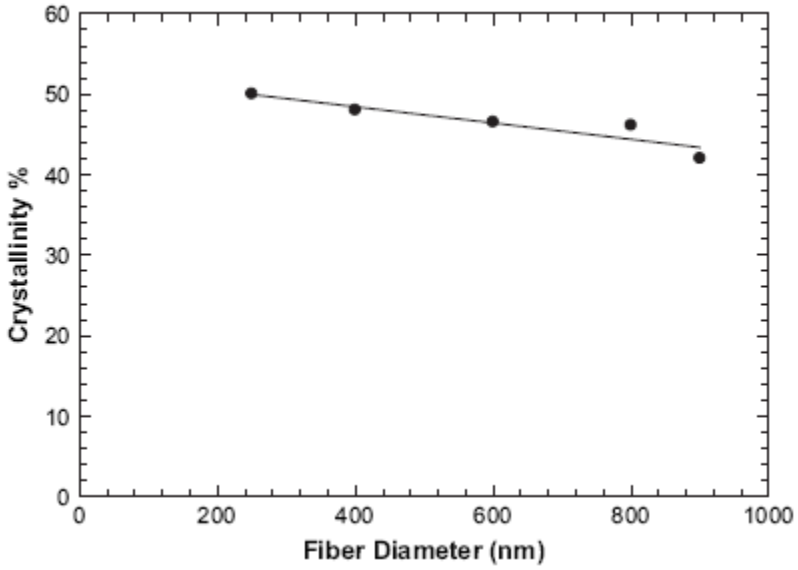

Figure 2.12 Plot of crystallinity vs. fiber diameter for aligned fibers [85].

Curgul [132] verified the phenomenon that the molecules, in nanofibers, are preferentially oriented parallel to the surface. The mobility of the chains at the skin is higher than the mobility of the chains in the core region [133, 134]. Therefore, the chains

at the skin are easily oriented under the influence of electric field. Furthermore, the crystallites are disoriented with respect to the fiber axis.

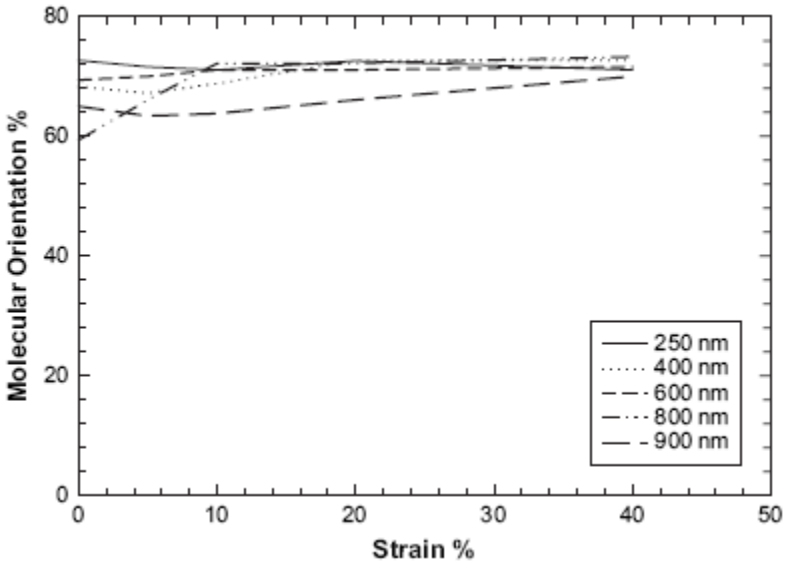

Figure 2.13 Plot of molecular orientation vs. strain for aligned fibers with different diameters [85].

When the fiber diameter decreases, the size of the skin region becomes analogous to the overall diameter of the fiber at a critical diameter [86]. Wong et. al. established a relationship between the microstructure of the PCL fibers and their diameter [85]. WAXD was used to determine the degree of crystallinity and molecular orientation in the fibers. Figure 2.12 shows the degree of crystallinity vs. the fiber diameter. Figure 2.13 shows the molecular orientation vs. strain for different fiber diameters. The degree of crystallinity and molecular orientation determined increase with decreasing the fiber diameter. Hence, it is concluded that as fiber diameter is reduced, there is an enhancement in the alignment of the molecules in the direction of fiber axis.

2.3.3.4. Effect of Collector on Structural Properties

The type of collector and the TUV of the drum/disk collector selected could influence the isotropic or anisotropic alignment of the fibers along with the crystal morphology and molecular orientation [121].

Kongkhlang [121] shows that when a rotational collector is used, the polymer chains in the crystalline regions can be drawn further in the draw direction compared to the polymer chains in the nonwoven fabrics that are obtained using a stationary collector. The force due to the rotational speed of the collector along with the shear force and elongation force may contribute to the alignment of the polymer chains in the direction of the fiber axis. Thus, it is expected that the crystalline orientation in the fibers improves with the speed of the collector [135]. The use of high speed rotational collectors leads to the "fanning" effect and the evaporation of the solvent is much quicker compared to the stationary collectors [136]. The speed creates a high-viscosity environment for the polymer chains in the electrospinning jet. It also leads to the transfer of the tensile stress onto the polymer chains during the fiber deposition. Thus, the crystallization in the fibers occurs due to the "sliding mechanism" and results in extended chain crystals [136]. Furthermore, as the rotational force contributes towards the stretching of the polymer jet, hence as the rotational speed is increased, the diameter of the fiber decreases. This explains the ordering of the crystals at higher collector speeds. From the other side, when the static parallel electrodes are used for obtaining aligned fiber arrays, the extended chain crystals are not observed and the crystal orientation is expected to be inferior compared to rotational collectors.

2.3.4. Mechanical Properties of Electrospun Fibers

Polymer electrospun nanofibers have been proved to acquire exclusive mechanical properties. For instance, the mechanical deformation behavior of the fibers is unique and can be radically dissimilar from their macroscopic versions [85, 112, 128, 136, 137].

2.3.4.1. Effect of Structural Morphology on Tensile Properties

The tensile properties of the fibers are affected by the crystalline and amorphous phases present in the fibers. During electrospinning, changes in the structural formation taking place in fibers, especially crystallinity and molecular orientation, pass on the physical properties to the material and play a vital role in deformation behavior of the fibers [85-88]. Hence, possessing a better knowledge of the intrinsic structures is essential for understanding their influence on mechanical properties. The amorphous phase of the fibers provides the elastomeric properties and the crystalline phase imparts dimensional constancy to the array of molecules.[85] For this reason, the mechanical deformation characteristic of the fiber is affected by the ordered or random arrangement of the crystalline and amorphous phases in the fiber [85-88, 121, 122].

Curgul et al. [132] argues that the mechanical properties of the fibers are influenced by the properties of the core and skin region of the fiber. The mass density at the core region of the fiber is comparable to the bulk density of the polymer. Therefore, the core region of the fiber exhibits bulk-like structure and physical properties. From the other side, the property exhibited by the surface region is entirely different. This is attributed to the major lower density and increased mobility of the chains at the surface of

the fiber in comparison to the core region [133, 134]. Hence, the overall mechanical property of the fiber is determined by the number of oriented fragments present at the surface of the fiber. Arienstein et. al. [86] also determined that the orientation of the amorphous chains in the supramolecular region of the fibers affects the deformation process of the fibers. By applying the latter finding to the study of the effect of fiber diameter on tensile strength, it should result in an abrupt shift in properties when decreasing the fiber diameter.

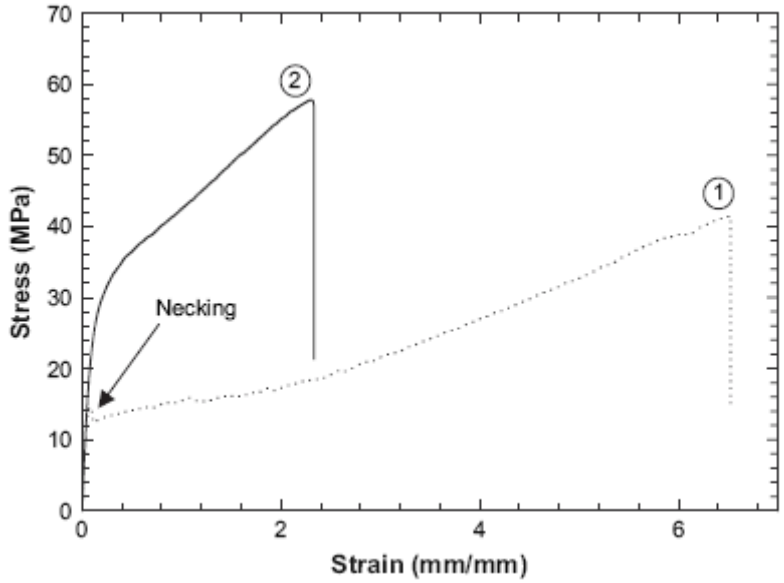

Figure 2.14 Representative stress-strain curves obtained from the tensile tests performed on electrospun PCL and non-spun PCL samples. Curve 1 represents the electrospun sample and Curve 2 represents the non-spun sample [85].

That is because the effect of fiber skin on the overall nanofiber becomes increasingly dominant as (1) the fiber surface dimension approaches the radius of gyration of polymer chains, thus constraining segmental motion, and (2) the fiber core diminishes when

decreasing the fiber diameter. Wong et. al. [85] evaluated the effect fiber diameter on the tensile properties. The tensile properties of the fiber were compared with the tensile properties of bulk polymer system prepared using injection molding. Figure 2.14 shows the schematic of stress-strain curves for spun and bulk samples. There is a significant difference in tensile strength and tensile behavior displayed by both systems. Stress-strain curves of electrospun sample did not exhibit a necking phenomenon whereas the bulk sample displayed a necking phenomenon. This is credited to the oriented and stretched polymer chains in the fibers [138, 139]. Similar results were seen by Lu and coworkers [138].

2.3.4.2. Effect of Collector Type on Tensile Properties

The type of collector used for collecting electrospun fibers could have a noticeable effect on the tensile properties of the fibers. The two most famous collectors are the stationary and the rotational collectors.

A. Stationary Collector

The tensile properties of the fibers collected using this method depend greatly on the degree of alignment of the fibers within the mat, fiber lay-ups and interface properties of fiber-fiber contact [96, 116, 138]. Usually, the tensile properties of the nonwoven fabrics are lower than the mats with uniaxially oriented fibers. This is due to the highly porous nature of the nonwoven fabrics. Furthermore, during the tensile loading, only the fibers oriented along the loading direction are exposed to the stretching force, while the fibers oriented perpendicular to the loading direction do not experience the stretching force.

B. Rotational Collector

The macroscopically aligned fibers obtained using a rotating disc collector are found to have anisotropic properties [140, 141]. The tensile strength and modulus have been proven to be higher than the ones of randomly oriented fibers [141]. Because the molecular chains in the fibers are aligned along the fiber axis, which is in the direction of the loading, the samples exhibit enhanced tensile properties.

Table 2.4 Tensile properties of PLLA single nanofibers electrospun at TUV of 63 and 630 m/min [9].

b

Table 1. Tensile properties of electrospun PLLA single nanofibre.

Conditions	Mw ($g\ mol^{-1}$)	Take-up velocity ($m\ min^{-1}$)	Fibre diameter (nm)	Tensile modulus (GPa)	Tensile strength (MPa)	Strain at break (%)
Electrospun fibres	300 000	63	890 ± 190	1.0 ± 1.6	89 ± 40	1.54 ± 0.12
		630	610 ± 50	2.9 ± 0.4	183 ± 25	0.45 ± 0.11
Melt-spun fibres [27]	212 450	600	34 000	3.9	192	2.2

The tensile properties of the aligned fiber array samples also depend on the technique used to collect aligned fiber arrays. The fibers tend to have uniform morphology and diameter at higher rotational speeds which contributes towards the tensile properties of the samples [109-117].

Besides, other researchers determined that the tensile modulus and strength increase with the TUV while the elongation at break decreases [3, 9, 18]. Table 2.4 shows the variation of the tensile modulus and strength and the elongation at break with the TUV. For nylon 6, it is vital to note that the α-form crystals have a higher Young's modulus than the γ-form crystals [17, 81, 82].

C. Effect of Fiber Diameter on Tensile Properties

The mechanical properties of the fiber mats are significantly influenced by (1) fiber structure, (2) geometrical arrangement of the fibers, (3) individual fiber properties and (4) interaction between the fibers. These properties are thorny to control during the electrospinning process. Therefore, it is important to determine the mechanical properties of a single fiber. Recently, researchers determined the tensile properties of single fibers and showed that the size of the fiber affects its tensile properties. It is proved by researchers that, when the diameter of the fiber is reduced below the critical diameter, the tensile properties are enhanced [85-88]. Arinstein et al. [86] demonstrated that this phenomenon occurs when the size of the supramolecular structures of the fibers is analogous to the overall fiber diameter. The orientation of macromolecules present in the supramolecular structures of the amorphous phase plays a governing role in increasing the mechanical properties of the fibers. Upon increasing the fiber size, both the tensile strength and modulus decrease and the larger diameter fibers have a propensity to display bulk-like properties. This observation is important for the plausible applications of the eletrospun nanofibers. Instead of merely considering these polymers as fibers, they could be treated as miniaturized high aspect components for sensors and devices. Being aware that a sudden change in properties occurs as the diameter decreases proposes that we cannot employ acquired measurements from bulk specimens for modeling devices at the nanometer scale level. The modulus or tensile strength of fibers with a diameter greater than 2 μm is not affected by electrospinning and could be treated as bulk-like properties. The enhanced properties of finer diameter fibers were credited to the gradual ordering of the molecular chains and modest increase in the crystallinity of the fibers. The size effect

can also be attributed to the densely packed lamellae and fibrillar structures. In finer diameter fibers, the lamellae and fibrillar structures align themselves along the fiber axis, which plays a crucial part in enhancing the mechanical properties of fibers. The fibrillar structure possesses a high degree of molecular orientation and provides high resistance to axial tensile force.

2.3.5 Electrospun Fibers Applications

Fibers obtained from electrospinning have been showing unique mechanical, thermal, chemical and electrical properties. Hence, they are used in several applications including tissue engineering, electrospun fiber reinforced composites, electrospun conductive fibers, and filtration.

2.3.5.1. Tissue Engineering Application

Ultra-fine fibers electrospun from biodegradable polymers have found potential applications in tissue engineering due to their high surface area to volume ratios and high porosity of the fibers [89, 92, 137, 142]. Furthermore, the option of seeding stem cells and human cells on the fibers renders electrospun materials an ideal candidate for tissue engineering applications [143, 144]. These fibers could be used to design structures which not only mimics the properties of the extracellular matrix (ECM) but also possesses high strength and high toughness properties. Other advantages of using electrospinning as processing technique for scaffold fabrication are cell compatibility and proliferation [145, 146]. This suggests a more thorough understanding of the mechanical behavior of electrospun nanofibers is essential. For example, the fracture toughness of

the synthetic electrospun scaffolds has not been addressed at all and this is a decisive factor for assessing the mechanical integrity of the scaffolds. Due to their hierarchical structural arrangement, the natural tissues possess superior fracture toughness values compared to any of the synthetic scaffold materials that are currently used [147]. In an attempt to match the mechanical properties of natural composites, the designed scaffolds should mimic the architectural design used by natural tissues.

2.3.5.2. Electrospun Fiber Reinforced Composites

Although electrospun fiber reinforced polymer composite possesses a potential for developing high strength materials and materials with good thermal and electrical conductivity, a few studies have investigated the use of electrospun fibers in composite forms [93-95, 148].

The commonly used reinforcements in polymer matrices create stress concentration points due to their irregular shape geometries, and the cracks propagate by cutting through the filler or travel around the filler particle [94]. The reinforcing effect of the fibers and the interfacial adhesion between the fiber and the matrix material is influenced essentially by the size of the fibers used. The size of the fibers could be controlled and a smaller concentration of the fibers could then be used for efficient reinforcement. From the other side, the high percent of porosity and irregular pores between the fibers could lead to an interpenetrated structure when dispersed in a matrix, which also enhances the mechanical strength due to the interlocking mechanism. These characteristic features of the nanofibers better enable the transfer of applied stress to the fiber-matrix interface than most of the commonly used fillers [93].

Bergshoef et al [148] added 50-200 nm diameter electrospun nylon 4,6 fibers to an epoxy resin matrix. They found that the composite stiffness and the strength become considerably higher than the matrix material properties. Fong [93] used nylon 6 fiber reinforced composite for dental applications. The flexural strength and elastic modulus of the fiber reinforced composite notably increase with relatively small amount of fiber content (~ 5 wt%).

The dispersion of the fibers in the matrix and the control of fiber orientation in the matrix material are the current issues associated with the use of electrospun nanofibers as reinforcement materials. The fracture toughness and fracture energy of the composite rely on the alignment of the fibers in the composite [95]. In order to achieve better reinforcement, the electrospun nanofibers may need to be collected as a highly aligned yarn instead of being randomly oriented. The dispersion of the electrospun mats in the matrix could be improved if the fibers are trimmed into shorter fragments. Hence, the electrospun fibers must be collected as aligned bundles instead of nonwoven system.

2.3.5.3. Electrospun Conductive Fibers

Electrospinning has found applications in manufacturing flexible and compliant conductive nanofibers for miniaturized devices [114, 149, 150]. Researchers seek to develop compliant electrodes for electroactive polymer actuators. The use of electro-spinning to produce fibers from conductive polymer matrices can be useful for these applications. Moreover, electrospinning can be used to disperse the carbon nanotubes (CNT) in the fibers for improving the mechanical, electrical and conductive properties of

the matrix [90, 91]. Due to the sink flow mechanism, the CNT have a propensity to orient along the fiber axis and are embedded in the fiber core.

2.3.5.4. Filtration

Electrospun fibers with micrometer-sized diameters have found potential applications in the filtration industry [114, 151-153]. The electrospun fabrics used for such applications present the advantages of high surface area to volume ratio, low air resistance, lower filter mass and the flexibility of adding surface functionality on the fibers by blending or by incorporating nanofillers [152]. Electrospun fibers have been investigated for aerosol filtration, air cleaning applications in industry and for particle collection in clean rooms. Basically, aerosol particles are filtered due to the electrostatic attraction present between the filter media and aerosol particles. Electrospun fibers used in the filtration media could offer a higher efficiency of filtration as the static charge used to produce the electrospun fibers have the capability of remaining in the fibers and thus help in the filtration of aerosol particles. It is been shown that the filtration efficiency of the electrospun mats is as good as the commercially available filters but the advantage lies in the filter mass. The filter mass of the electrospun fibers is considerably lower than the commercially available filter [114, 153].

CHAPTER III

EXPERIMENTAL WORK

3.1. Material

The studied material is nylon 6 which was purchased from Sigma Aldrich CAS 25038-54-4 and has a density of 1.084 g/mL. The solvent is formic acid (88%) which was purchased from EMD Corporation CAS 64-18-6.

3.2. Collection of Aligned Electrospun Fibers

Nylon 6 pellets were dissolved in formic acid where the solution was magnetically stirred overnight. A syringe pump was used for generating a pressure to maintain a solution drop on the tip of a 0.559 mm (Gauge 21) stainless steel needle. The needle was attached to a 5 mL capacity syringe filled with solution. The length of the needle's channel was 25 mm. The flow rate of the polymer solution was 2 µL/min. The needle was charged with a high voltage of 20 kV. The gap distance between the tip of the needle and the top of the collector was set to 150 mm. The electrospinning of the fibers was done at room temperature. The fibers were dried in vacuum at 100°C overnight prior to testing, a method mentioned by other researchers [154], to vaporize any remaining formic acid which has a boiling point of 100°C. Figure 3.1 shows a detailed schematic of the electrospinning setup. More precisely, the rotating disc collec-

tor, shown in Figure 3.2 (a), had a diameter of 150 mm. A copper tape was uniformly added from the middle of the disc up to the surface, in order to have a uniform distribution of the current on the surface of the disc.

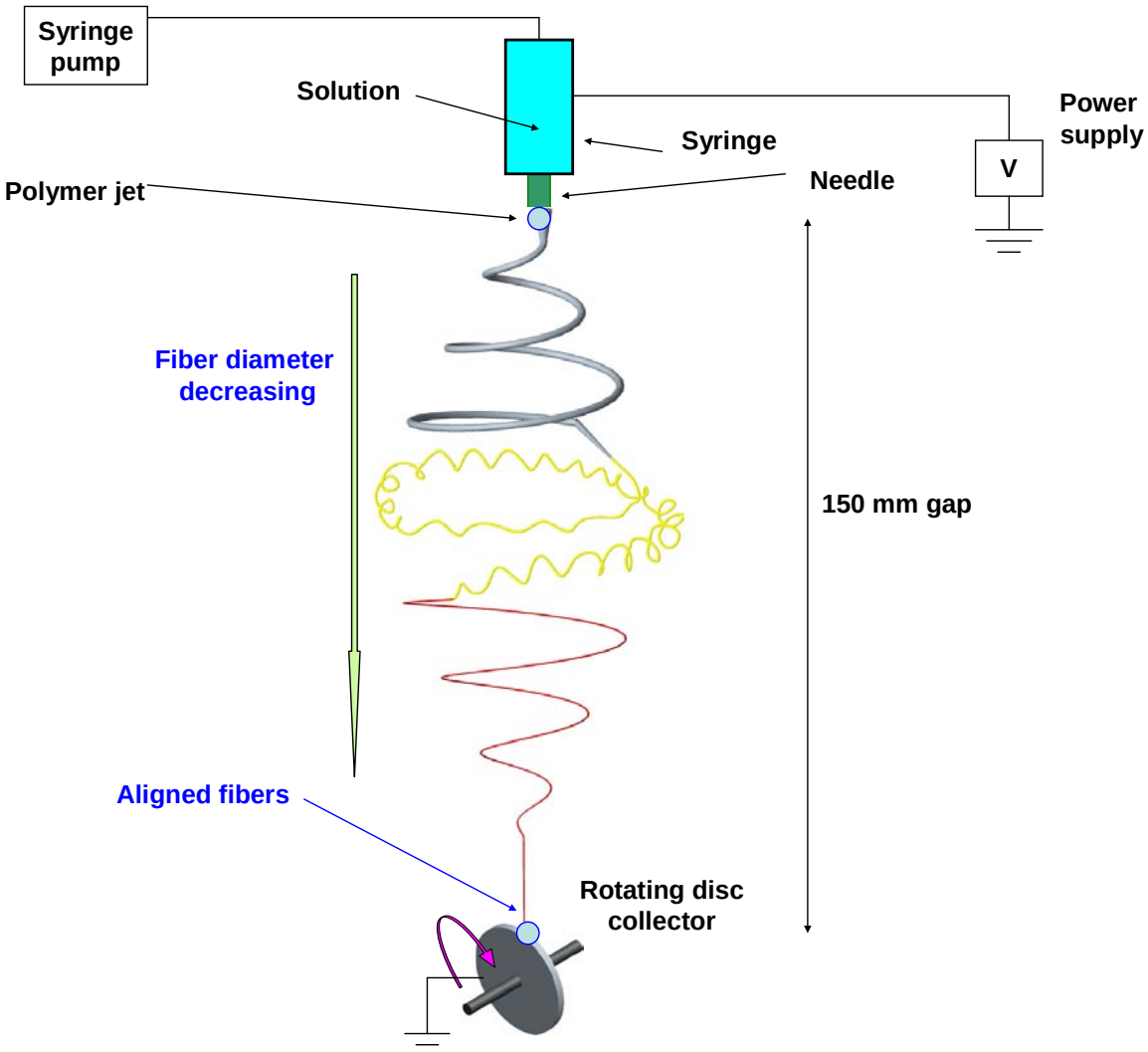

Figure 3.1 Schematic of the electrospinning setup for the formation of fibers and adopted trajectory before depositing in an aligned fashion on the rotating disc collector.

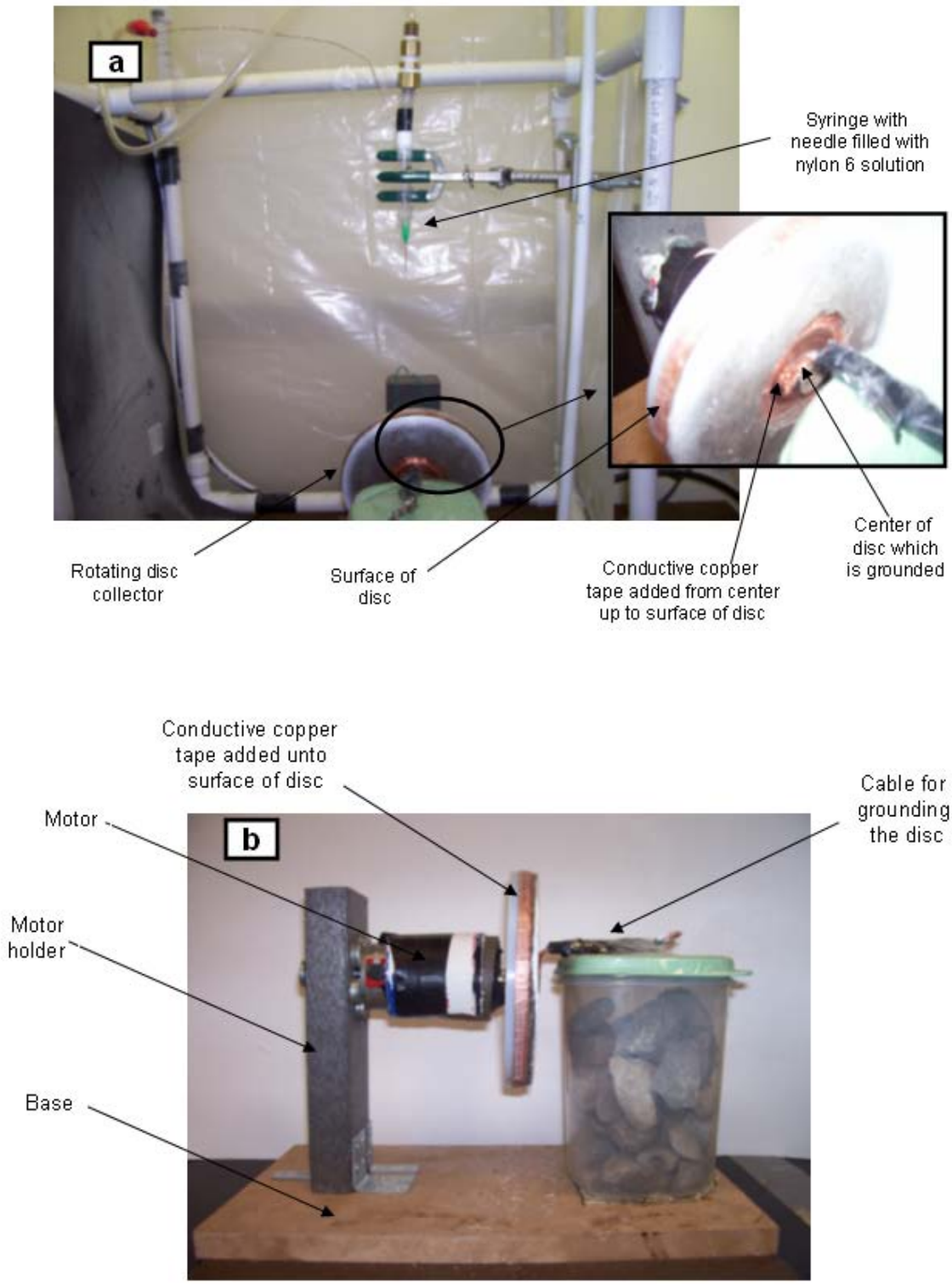

Figure 3.2 Electrospinning setup in our lab (a) for collecting aligned fibers and (b) represents a side view of the disc.

Also, a 10 mm wide one-sided conductive copper tape was added on the surface of the disc in order to make it conductive.

3.4. Differential Scanning Calorimetry

The T_m of the fibers was determined using TA Instruments 2920 modulated DSC at a heating rate of 10°C per minute from -110 to 245°C under a dry nitrogen atmosphere. Hermetic pens were used with a sample weight of 2 mg.

3.5. X-Ray Diffraction Analysis

The crystallographic structures, molecular and crystalline orientation, and degree of crystallinity were investigated using two dimensional (2D) WAXD. The 2D WAXD patterns were obtained using a Rigaku X-ray imaging system with an 18 kW rotating anode X-ray generator in the transmission mode. Each sample had an average length, width, and thickness of 20, 2, and 0.15 mm, respectively. The X-ray hit the sample in a form of a circle having a diameter of 0.5 mm. Therefore, millions of fibers in the sample were subjected to the X-ray at the same time.

The degree of crystallinity was determined from the WAXD patterns using PEAKFIT software, following the method set by N. Rahman et. al. [155]. Furthermore, the molecular orientation was determined from the intensity vs. azimuthal angle scan, using the following formula [18]:

$$F = \frac{180° - \Delta\phi_{1/2}}{180°}$$

where $\Delta\phi_{1/2}$ represents the full width at half maximum (fwhm) of the azimuthally scanned peak.

The crystalline orientation was determined using the Herman's orientation function *f* which is defined as follows:

$$f = \frac{3\overline{\cos^2 x} - 1}{2}$$

where $\overline{\cos^2 x}$ is the average cosine squared value of the angle x between the stretching direction in the sample and the x crystallographic direction. $\overline{\cos^2 x}$ is determined from the following equation:

$$\overline{\cos^2 x} = \frac{\int_0^{\pi/2} I(x)\cos^2 x \sin x \, dx}{\int_0^{\pi/2} I(x)\sin x \, dx}$$

where $I(x)$ is the corrected intensity.

Thus, *f* could vary from a value of +1 for parallel orientation of the crystallite axis with respect to the stretching direction of the fiber, through a value of 0 for random orientation, to a value of -0.5 if the axis is orientated perpendicular to the stretching direction of the fiber [156].

The overall density of each sample was determined using the formula which is adopted by other researchers [17, 154]:

$$\rho = C_\gamma \times \rho_\gamma + C_\alpha \times \rho_\alpha + (1 - C_\gamma - C_\alpha) \times \rho_{am}$$

where C_γ and C_α denote the percentage of γ- and α-form crystals, respectively.

ρ_γ , ρ_α , and ρ_{am} represent the densities of the γ- and α-form crystals and the amorphous phase, respectively, where their values were reported in the background section. Also, ρ represents the overall density of the sample.

3.6. Mechanical testing

An Instron 5582 tensile testing machine with a load cell of 500 N was used to perform the tensile testing. A testing method used by other researchers was adopted to conduct the testing [154]. Figure 3.3 shows a schematic of the tensile test setup. The tested fibers had a length of 15 mm and were stretched at a strain rate of 1.12 mm/min. The weight of the specimen was measured using a weight balance having an accuracy of 0.1 mg. Fibers were examined under the SEM to check the alignment: more than 99% of the fibers were uniaxially aligned. The number of fibers was determined using the following equation:

$$N = \frac{4 \times M}{\rho \times \pi \times D^2 \times L}$$

where N is the number of fibers, M the mass of the fiber specimen (g), ρ is the density of nylon 6, in g/m^3, determined through WAXD analysis, *D* the fiber diameter (m), and *L* the fiber length (m). Specimens containing an average of six million aligned fibers were tested simultaneously as one sample. Shown below is a detailed calculation for obtaining the number of fibers in each specimen.

For a specimen of mass $M = 2.5 \times 10^{-3}(g)$, a diameter $D = 180 \times 10^{-9}(m)$,

$\rho = 1.1 \times 10^6 (g/m^3)$ and a length $L = 15 \times 10^{-3}(m)$, we obtain:

$$N = \frac{4 \times 2.5 \times 10^{-3}}{1.1 \times 10^{6} \times \pi \times \left(180 \times 10^{-9}\right)^{2} \times 15 \times 10^{-3}}$$

Hence:

$N = 6 \times 10^{6}$ fibers.

Three specimens were tested for every TUV. Each specimen required a load between 6 and 8 N for failure.

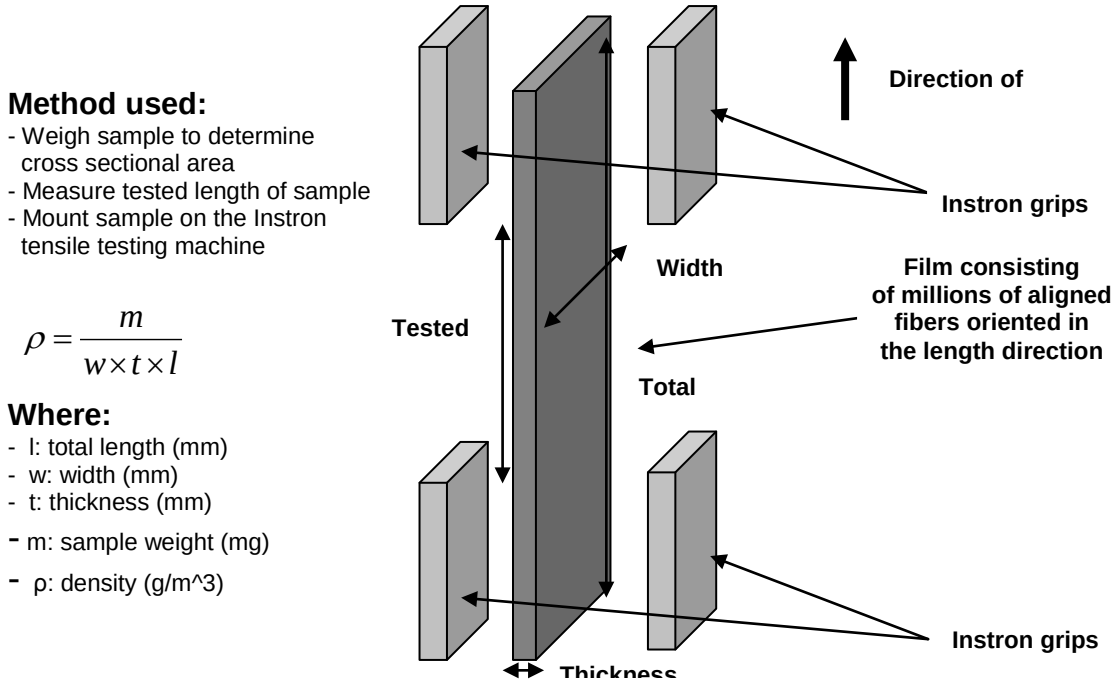

Figure 3.3 Schematic of the tensile testing setup for the fiber films [154].

3.7. SEM Analysis

The SEM instrument was used to study the morphology of the aligned and non-aligned electrospun nylon 6 fibers. In order to do so, a method was developed to collect

fibers that could be seen with the SEM. Then, the fiber diameter was measured and degree of fiber alignment determined.

3.7.1. Method for Collecting Aligned Fibers for SEM Analysis

Fibers were observed to sink in the adhesive in case being placed on a double-sided adhesive copper disc and subsequently could not be seen under the SEM. Therefore, fibers were placed on an SEM aluminum stub using two one-sided adhesive copper discs shown in Figure 3.4. The discs have a thickness of 0.2 mm. The first and second discs have a diameter of 10 mm and 7 mm respectively.

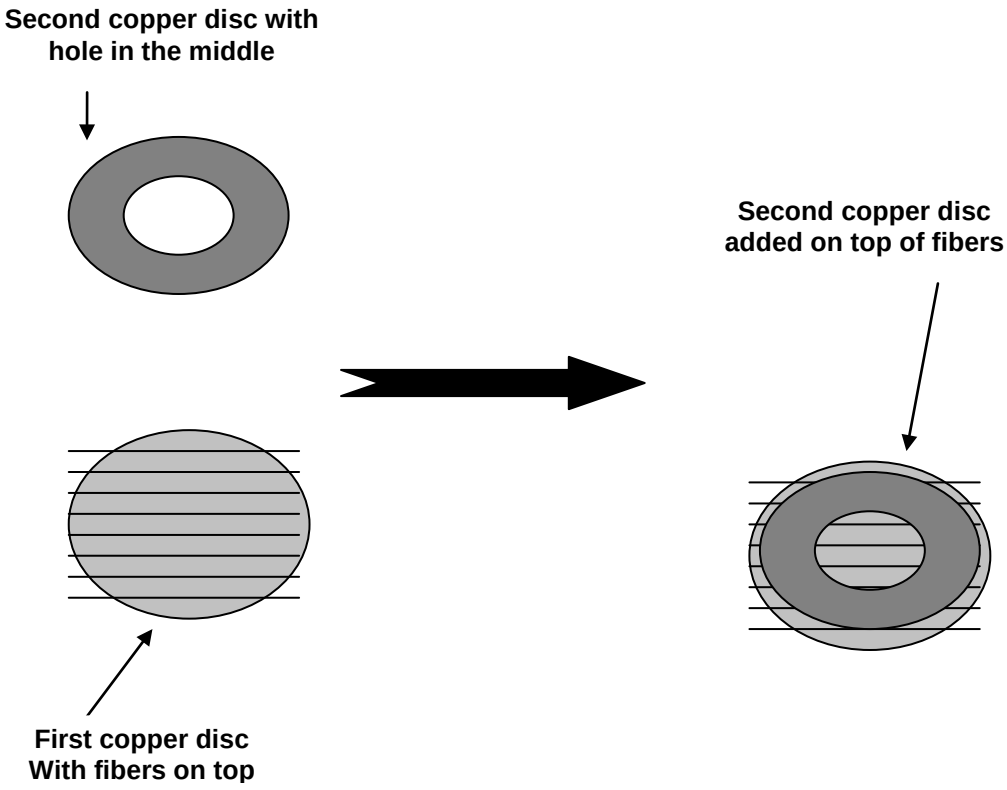

Figure 3.4 Schematic of the method used to prepare aligned fiber samples for SEM analysis.

The first disc was placed on the rotating disc collector to have fibers collected on its top surface. Then, the second disc, with a 0.4 mm hole in the middle, was added on top of the first disc which was covered with fibers. By doing so, the fiber alignment was preserved while being coated. The fibers were then silver coated using a K575x sputter coater for one minute at 55 mA in an argon-purged chamber evacuated at 500 mTorr. Then, the coated samples were examined with an accelerating voltage of 25 kV using a FEI Quanta 200 environmental SEM.

3.7.2. Diameter and Fiber Alignment Measurement

The fiber diameter was then measured using the SEM micrograph and "Image J" software. At least two hundred randomly selected fibers were chosen to obtain the average diameter and standard deviation.

To characterize the perfection of the parallel fiber alignment, the fiber orientation order parameter S was also measured using SEM micrograph and "Image J" software [15]. S is defined as follows:

$$S = \frac{3\overline{\cos^2 y} - 1}{2}$$

where y is the angle which the individual fiber forms with the preferred collection orientation.

3.8. DMA Analysis

The thermal transitions of the electrospun fibers were determined using DMA testing. The instrument used was Pyris Diamond DMA (Perkin Elmer-Seiko Instruments,

Boston, MA). The analysis of the samples was performed in tensile mode at a 1 Hz frequency. The samples were heated from -110 to 165˚C at 10 ˚C/ minute under nitrogen atmosphere. Figure 3.5 shows a schematic of the method used to mount the sample to the DMA. The fiber sample and film compression molded from bulk had a length of 2 mm and cross sectional area of 0.1 mm^2.

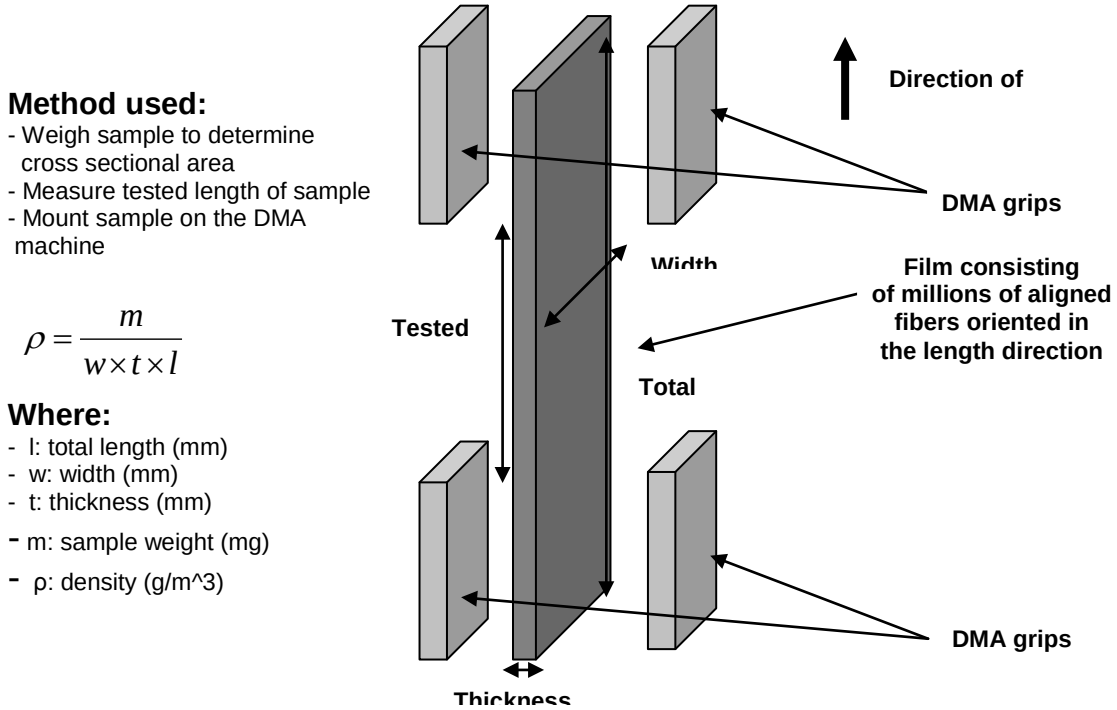

Figure 3.5 Schematic of the DMA testing setup for the fiber films.

CHAPTER IV

RESULTS AND DISCUSSION

4.1. SEM Analysis

The morphology of electrospun nylon 6 fibers was analyzed using the SEM. Figure 4.1 shows the SEM micrograph of nylon 6 electrospun fibers at a TUV of 14.2 m/s. It is obvious that the fibers possess a high alignment which is defined as the degree of orientation of the fibers in the direction of the arrow representing the draw direction.

Figure 4.1 SEM micrograph of electrospun fibers collected at a TUV of 14.2 m/s. The arrow shows a rough estimate of the average orientation of the fibers.

In order to determine the perfection of the fiber alignment, the fiber orientation order parameter S was calculated and determined to be 0.98 and remained almost constant with increasing the TUV. It has been reported that electrospun fibers do not exhibit a high alignment below a TUV of 12.5 m/s [7]. The average fiber diameter decreases with increasing the TUV as it is shown in Figures 4.2 and 4.3.

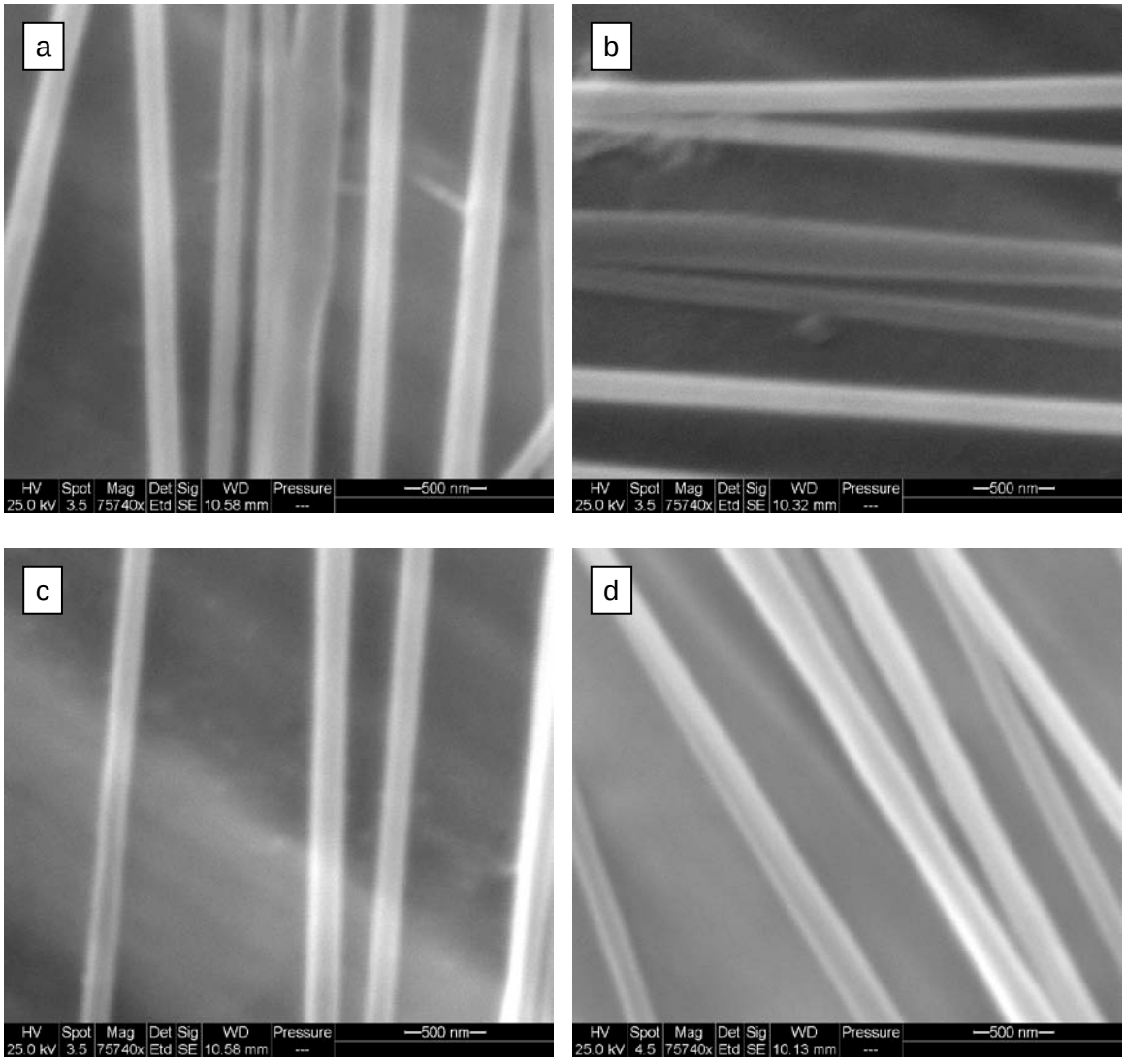

Figure 4.2 SEM micrographs of fibers collected at TUV(s) of (a) 14.2, (b) 17.8, (c) 19.6 and (d) 21.4 m/s.

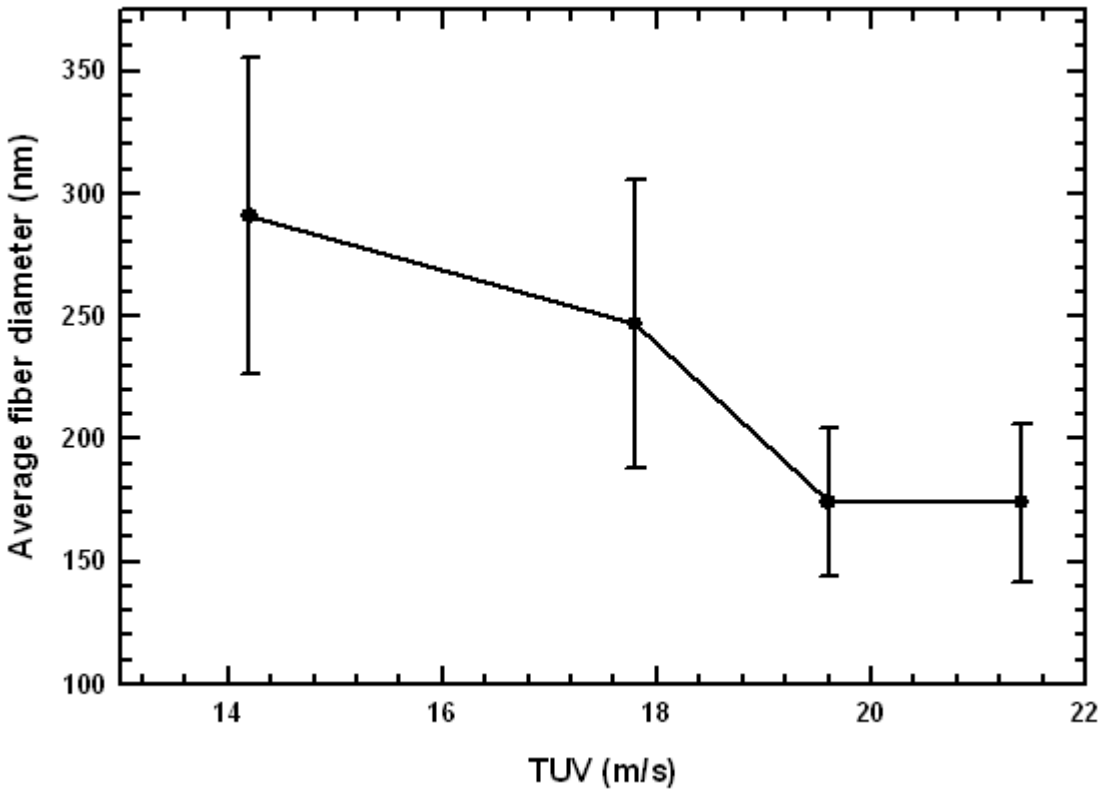

Figure 4.3 Plot of the variation of average fiber diameter vs. TUV.

That is due to the polymer chains being more stretched and aligned in the direction of the fiber axis. This part will be further discussed in detail in the WAXD section. These results are comparable to the ones obtained by Kotaki et. al. [18].

4.2. WAXD analysis

X-ray analysis was performed on aligned nylon 6 fiber layers for studying the variation of the molecular orientation, crystalline orientation, degree of crystallinity, and crystalline structure with TUV. The obtained 2D WAXD scans are shown in Figure 4.4 along with the one for a film compression molded from bulk.

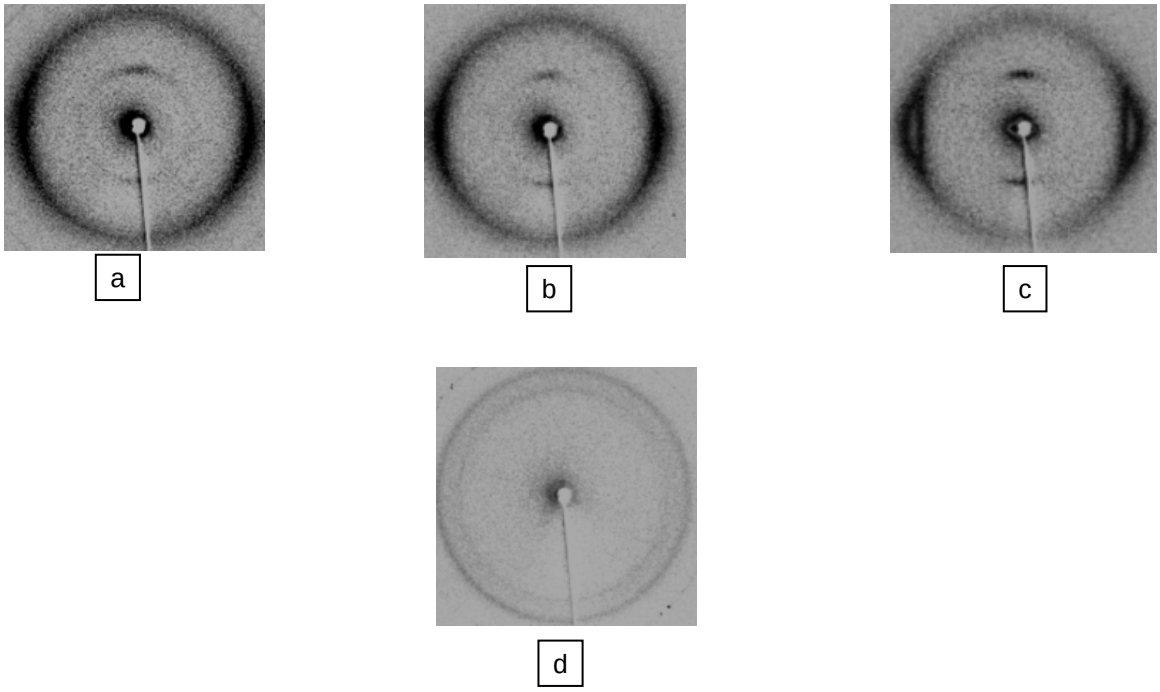

Figure 4.4 2D WAXD scans for (a) TUV of 14.2 m/s (b) TUV of 17.8 m/s (c) TUV of 21.4 m/s (d) sample compression molded from bulk.

The representative curves of the scan intensity vs. equatorial 2θ angle and azimuthal angle are shown in Figures 4.5 and 4.6, respectfully. Although electrospun at different TUV, all fiber samples have two obvious peaks at about 2θ = 11˚ and 22˚ as shown in Figure 4.6. These two peaks correspond to (020) and (200) lattice planes, respectfully, which shows that the γ-form crystals are present in the fibers. Further analysis on the plots was done at a later stage using PEAKFIT software for determining the amount of α-form crystals present in the sample. From the other side, the film compression molded from bulk has only two peaks at about 2θ = 20˚ and 24˚ as shown in Figure 4.6. These two peaks correspond to (200) and (002/202) lattice planes, respectfully. The absence of the peak at about 2θ = 1ĺ along with the latter results show that the α-form crystals are the only form of crystals present in the film compression mol-

ded from bulk. A summary of the obtained values of f, F, and S for different TUV(s) is shown in Table 4.1.

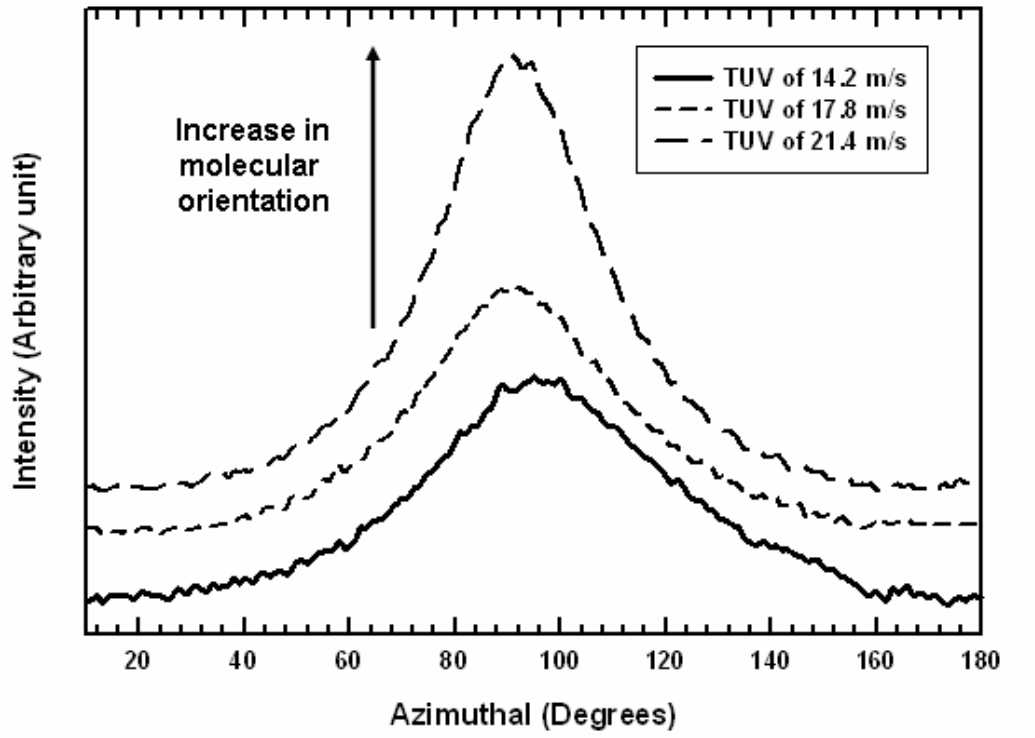

Figure 4.5 Representative curves of the 2D WAXD scan intensity vs. azimuthal angle for fibers samples collected at three different TUV(s).

The parameters f, F and S increased by 5.6%, 11% and 1% respectively with increasing TUV and with decreasing fiber diameter, as shown in Figures 4.7 and 4.8, respectfully. Therefore, it was concluded that molecular and crystalline orientation slightly increased with increasing the TUV. Similar results were obtained by other researchers [16, 18, 8]. However, the molecular orientation increased twice as fast as the crystalline orientation. That demonstrates that not only the orientation of crystalline phase increased in the fibers but also the one of the amorphous phase increased as well.

Table 4.1. Variation of molecular orientation, Herman's orientation, and fiber orientation order parameter with TUV.

TUV (m/s)	Molecular orientation function (Unitless)	Herman's orientation function (Unitless)	Fiber orientation order parameter S (Unitless)
14.2	0.72	0.89	0.98
17.8	0.77	0.91	0.99
21.4	0.80	0.94	0.99

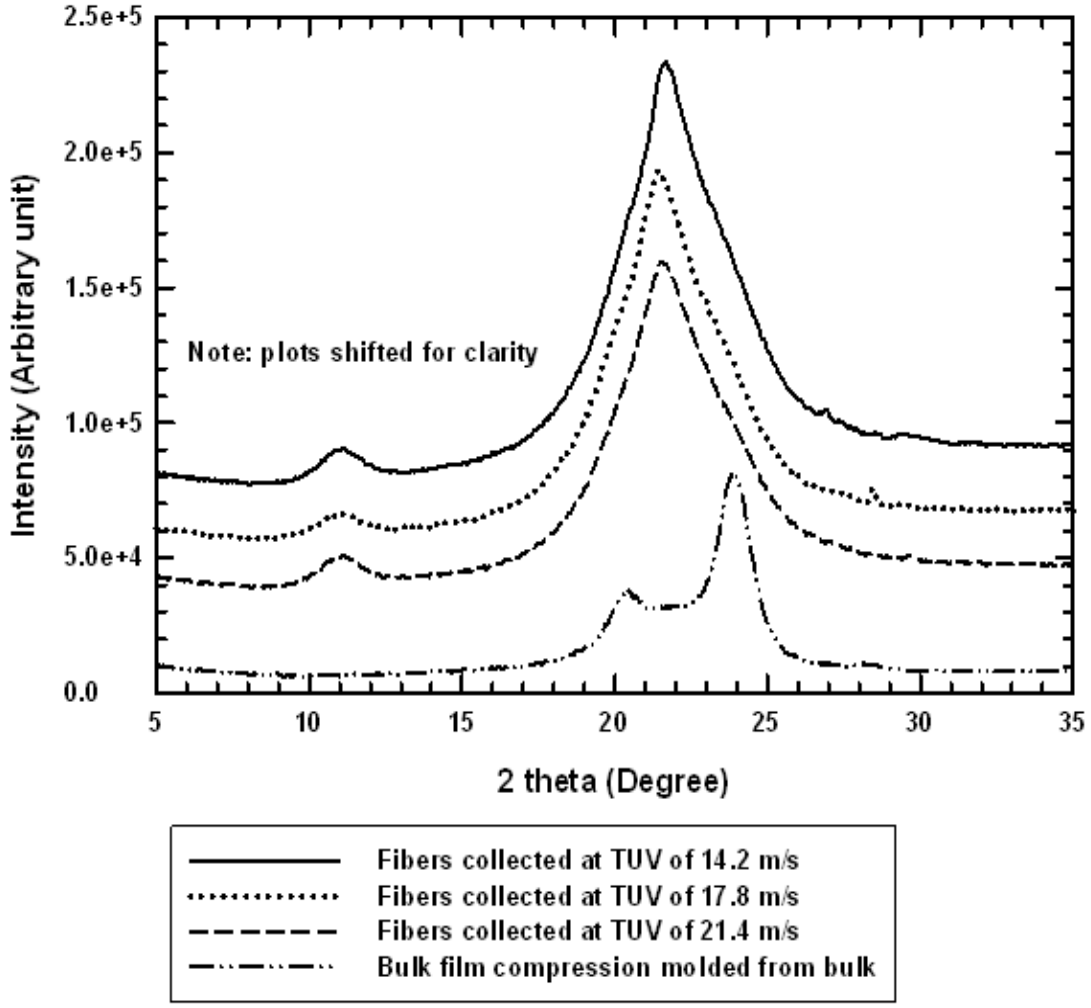

Figure 4.6 Representative curves of the 2D WAXD scan intensity vs. 2 theta angle for fibers samples collected at three different TUV(s) and also for sample compression molded from bulk.

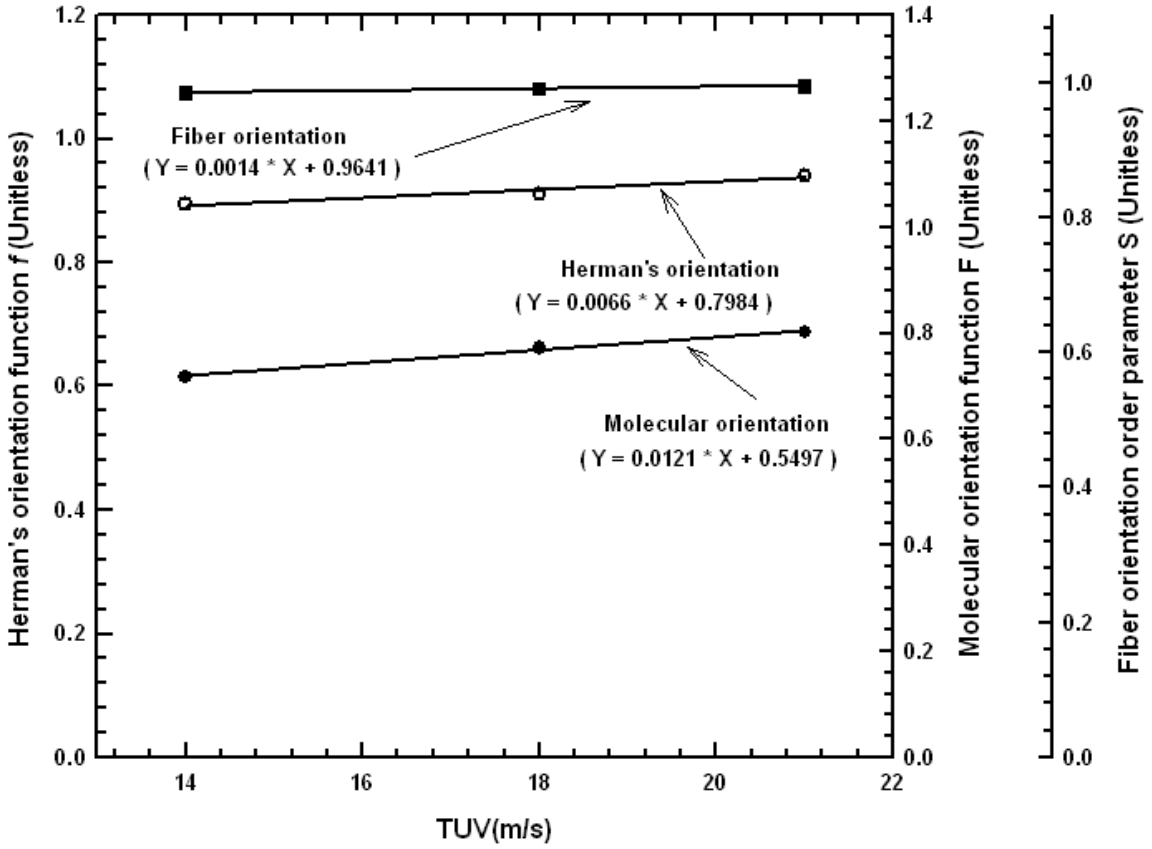

Figure 4.7 Plots of Herman's orientation function f, molecular orientation function F, and fiber orientation order parameter S vs. TUV.

PEAKFIT software was used to fit the individual peaks of the amorphous and crystalline phases in order to obtain the final peaks which match the ones obtained through the WAXD experiments. By doing so, the degree of crystallinity in the fibers was determined through the plots of the intensity vs. equatorial 2θ angle shown in Figure 4.6. Besides, the percentages of γ- and α-form crystals in the fibers were hence calculated. Figures 4.9, 4.10, and 4.11 show representative curves of the individually fitted peaks along with the final outcome peak compared to the original scan data for fibers collected at TUV(s) of 14.2 m/s, 17.8 m/s, and 21.4 m/s, respectively. A baseline was added for each plot before executing the program.

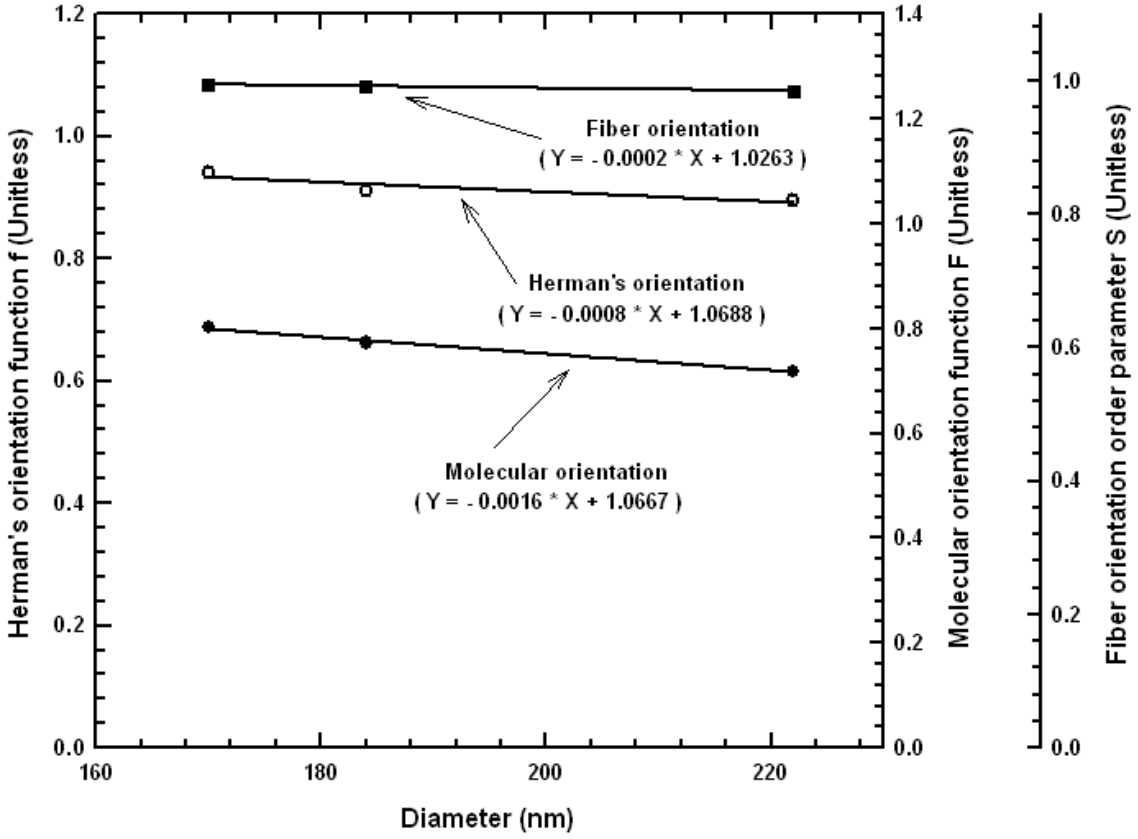

Figure 4.8 Plots of the variation of Herman's orientation function f, molecular orientation function F, and fiber orientation order parameter S with the average fiber diameter.

The peaks for the α-form crystals were taken at equatorial 2θ angles of 20˚ and 24˚ whereas the ones for the γ-form crystals were at equatorial angles of 20˚ and 24˚ whereas the ones for the γ-form crystals were at equatorial 2θ angles of 21˚ and 22˚. The amorphous peak was taken at equatorial 2θ of 22˚. Peaks for both crystal forms were kept at the same positions throughout the analysis for all plots.

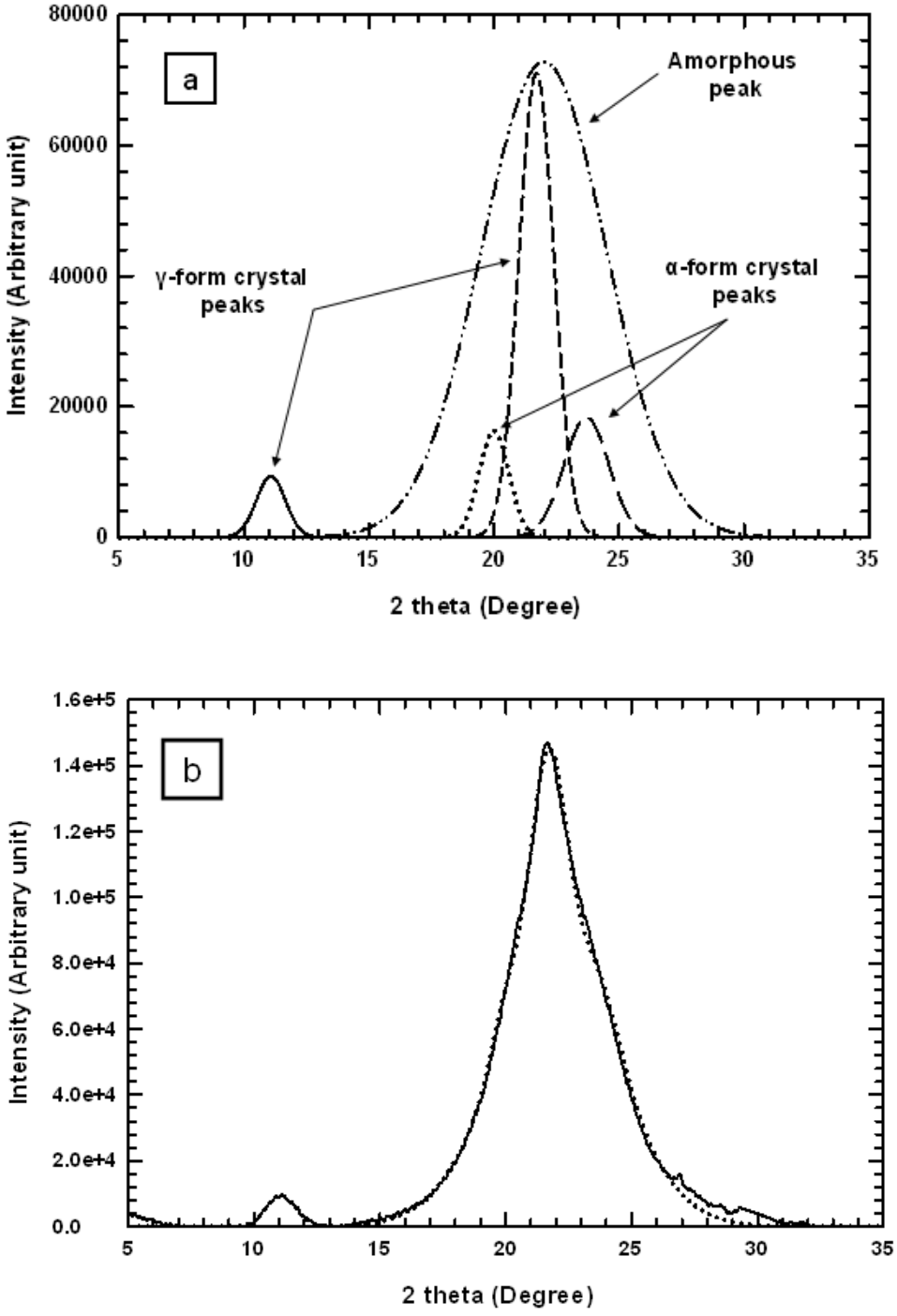

Figure 4.9 Representative curves of (a) the individually fitted peaks and (b) the final outcome peak compared to the original scan data for fibers collected at TUV of 14.2 m/s.

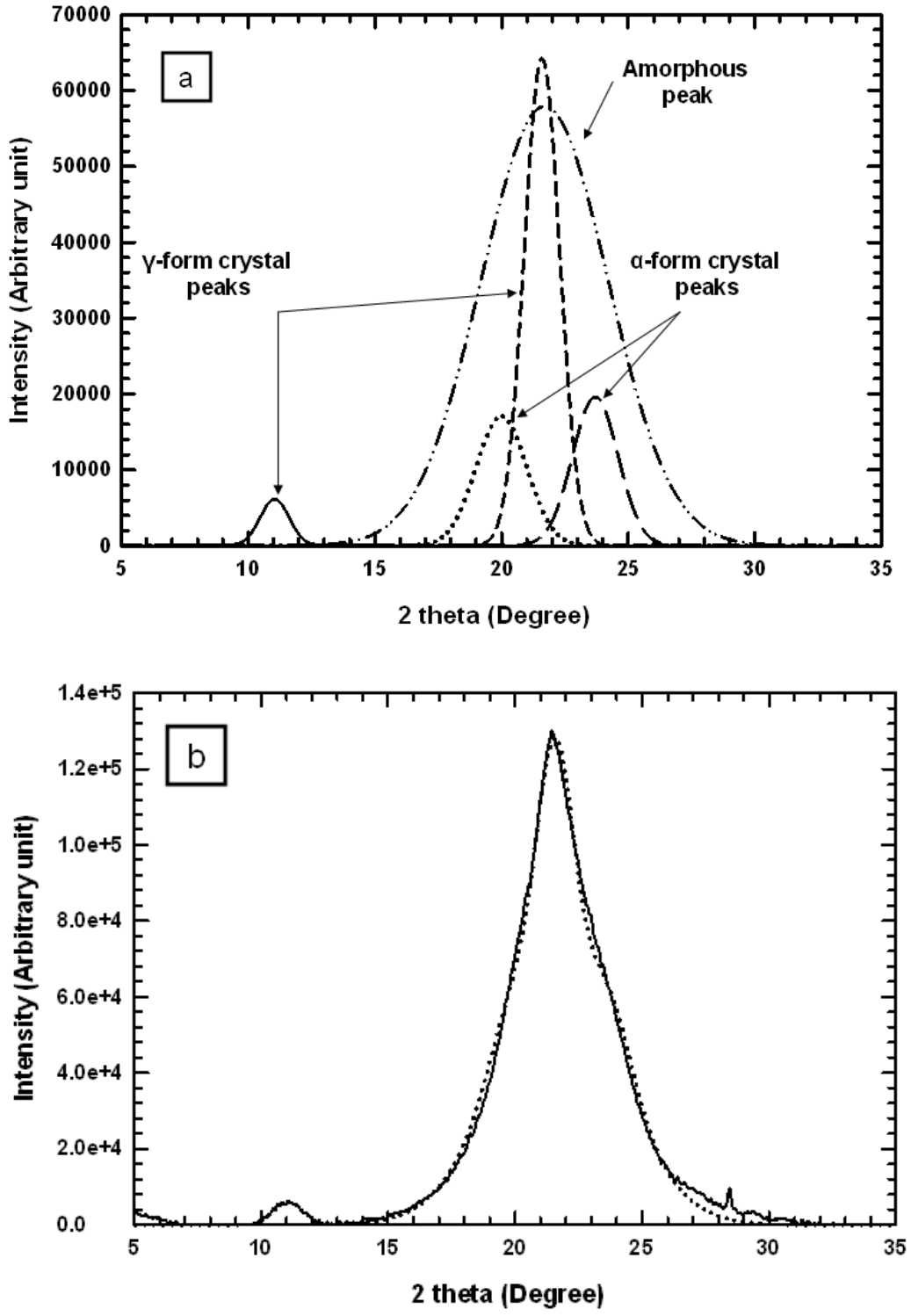

Figure 4.10 Representative curves of (a) the individually fitted peaks and (b) the final outcome peak compared to the original scan data for fibers collected at TUV of 17.8 m/s.

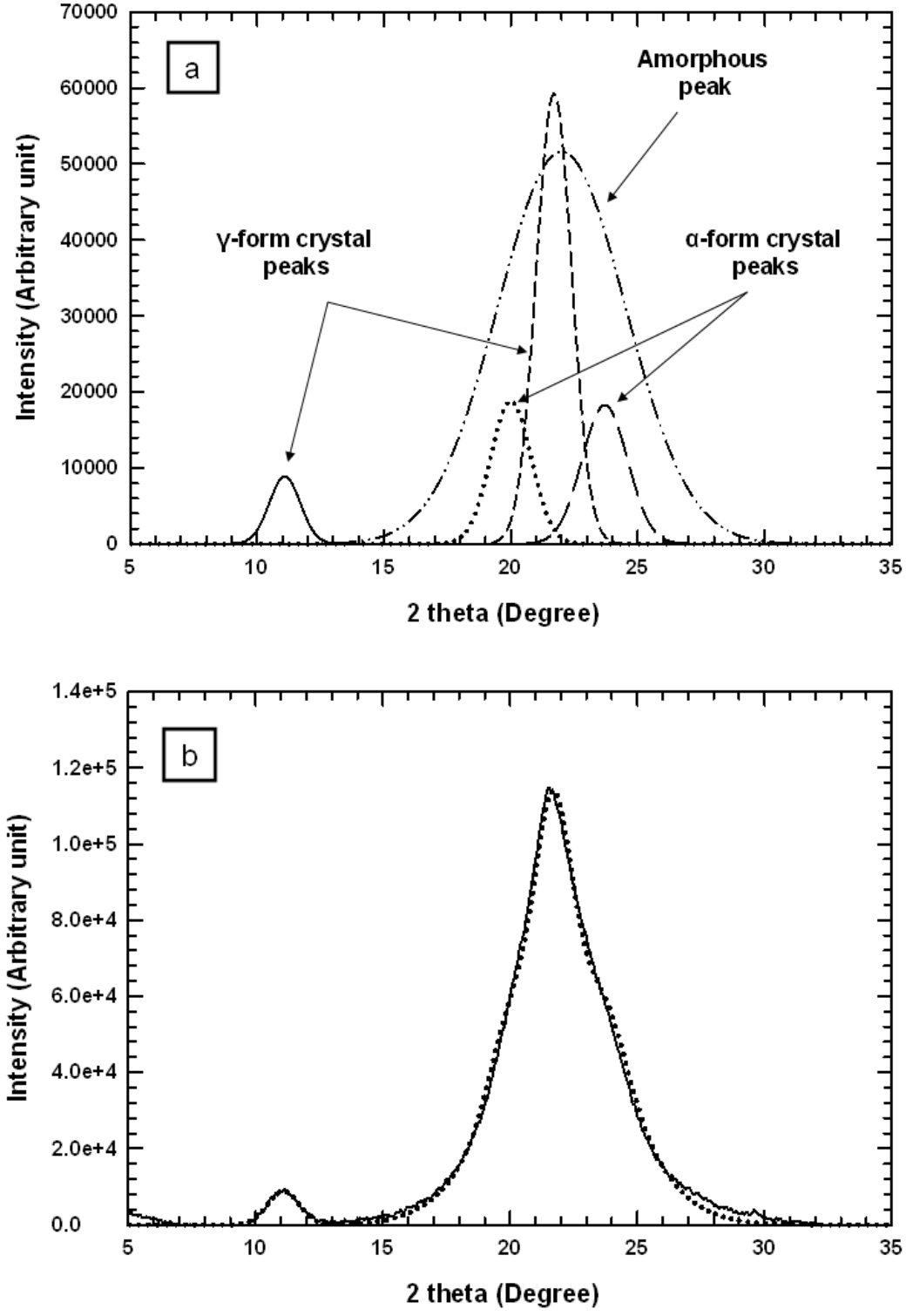

Figure 4.11 Representative curves of (a) the individually fitted peaks and (b) the final outcome peak compared to the original scan data for fibers collected at TUV of 21.4 m/s.

The final outcome peaks have a close match to the original scan data with an R^2 of 0.995. The obtained values for the degree of crystallinity are shown in Table 4.2.

Table 4.2 Variation of γ- and α-form crystals, crystallinity, and density with TUV.

TUV (m/s)	γ-form crystals (%)	α-form crystals (%)	Crystallinity (%)	Density (g/cm^3)
14.2	19.1	10.4	29.5	1.11
17.8	20.0	15.6	35.6	1.12
21.4	20.4	15.4	35.8	1.12

The variation of the degree of crystallinity with increasing the TUV and with decreasing the fiber diameter is shown in Figures 4.12 and 4.13, respectively.

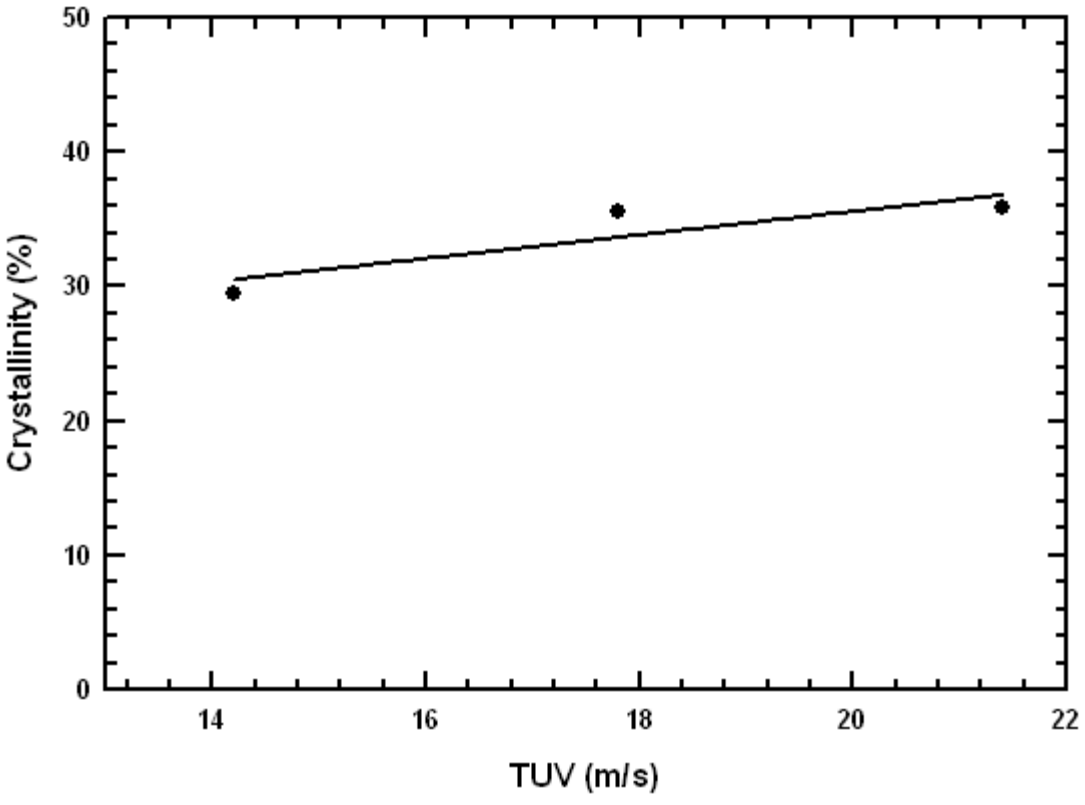

Figure 4.12 Plot of crystallinity vs. TUV.

It is palpable that the degree of crystallinity increased by 21% with increasing the TUV. At the same time, the percentages of α-form and γ-form crystals increased by 48% and 7% respectively. This proves that a more ordered crystalline morphology, α-form crystals, is being formed with increasing the TUV.

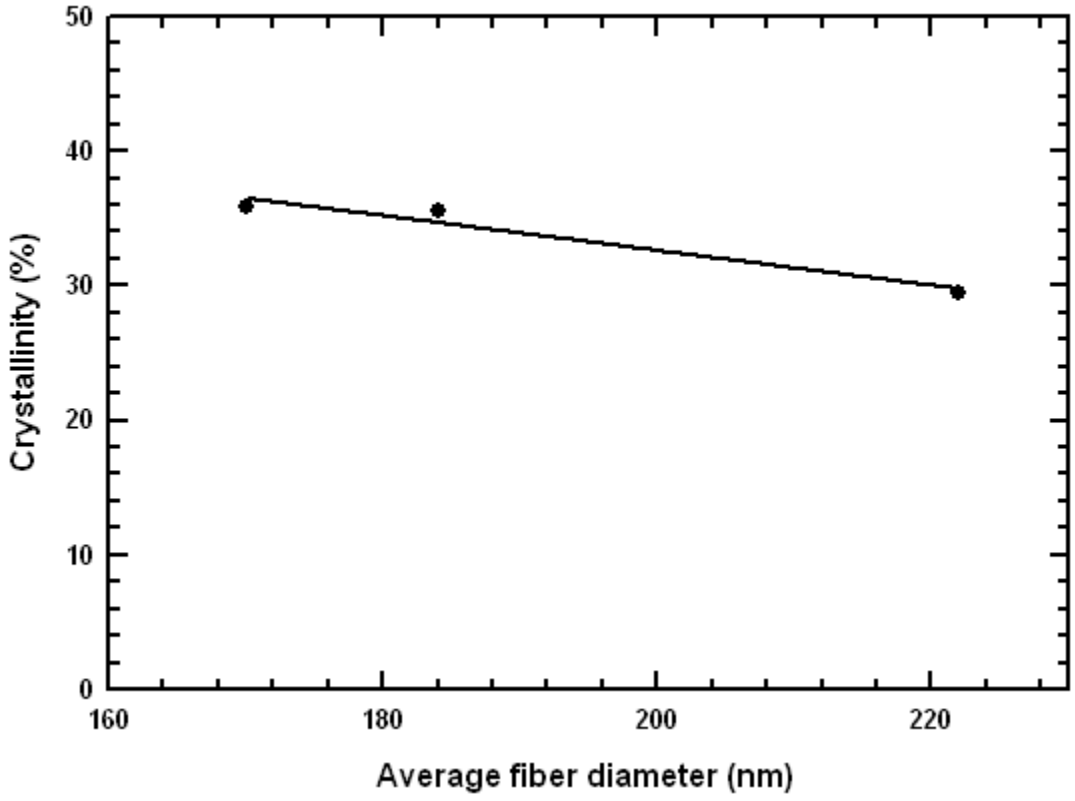

Figure 4.13 Plot of crystallinity vs. average fiber diameter.

4.3. Tensile testing

In order to study the effect of the TUV on their tensile properties, the nylon 6 fibers were subjected to tensile testing. Figure 4.14 through 4.17 show the representative stress vs. strain curves for different TUV values.

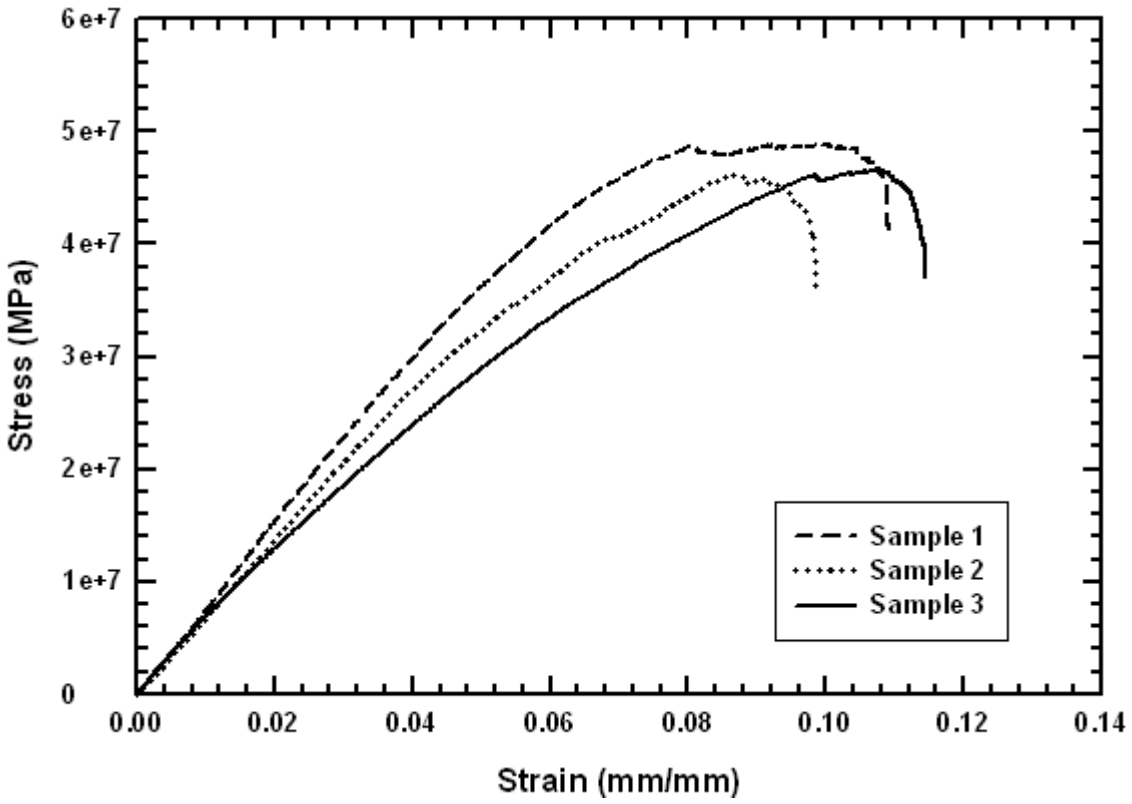

Figure 4.14 Representatives stress-strain curves for fiber films collected at a TUV of 14.2 m/s.

From the other side, Figure 4.18 shows the SEM pictures of tensile testing specimen which were taken for each of the four TUV values after the sample was subjected to tensile testing. From Figure 4.18, it is obvious that the nylon 6 remained in the form of a fiber after being subjected to tensile testing. Therefore, it is concluded that the millions of fibers which were subjected to tensile testing at the same time, regardless of the TUV at which they were collected, did not blend into each other becoming one bulk piece of nylon 6. Rather, the nylon 6 retained its characteristic as being in a fiber form. Therefore, the obtained tensile testing data could safely be used as being the data for nylon 6 in a nanofiber form. From the other side, Figure 4.19 shows the plot of the elongation at break vs. TUV for nylon 6 electrospun fibers.

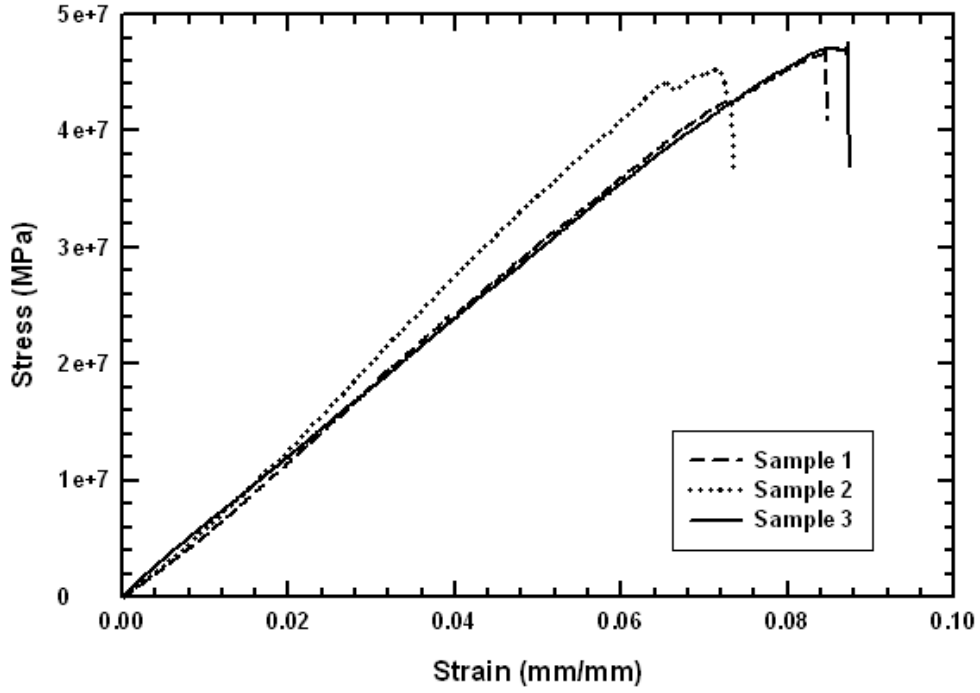

Figure 4.15 Representatives stress-strain curves for fiber films collected at TUV of 17.8 m/s.

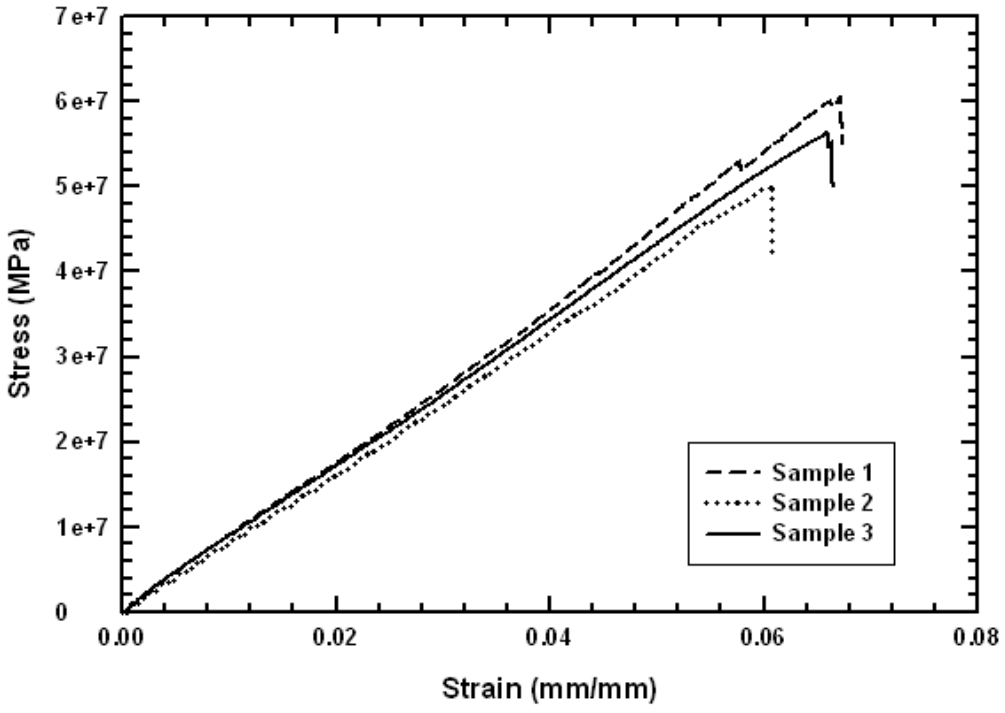

Figure 4.16 Representatives stress-strain curves for fiber films collected at a TUV of 19.6 m/s.

It is obvious from Figure 4.19 that the elongation at break decreases with increasing the TUV. In fact, the elongation at break decreases by 43.9 % with increasing the TUV from 14.2 m/s to 21.4 m/s, or in another word decreasing the average fiber diameter from 291 to 174 nm.

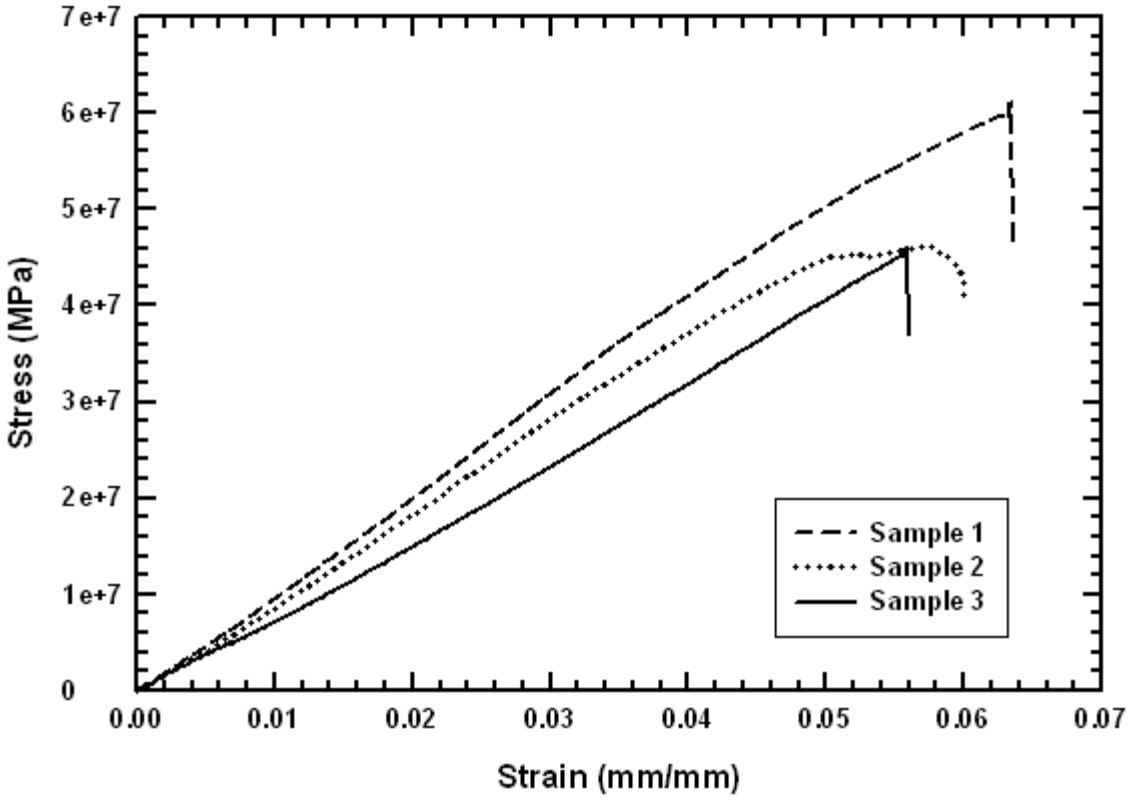

Figure 4.17 Representatives stress-strain curves for fiber films collected at a TUV of 21.4 m/s.

This phenomenon is proving that the decrease in fiber diameter is increasing the molecular orientation in the direction of the fiber axis and therefore enhancing the capability of the fiber to be less elongated. Figure 4.20 shows the plot of the tensile modulus vs. TUV. While the elongation at break decreases, the tensile modulus increases by 31.5%. This significant increase in tensile modulus is mainly due to the enhanced

effect of fiber diameter on the internal structure of the fiber where the percentage of α-form crystals increases. In fact, similar conclusions of improved molecular orientation and percentage of α-form crystals were also made at an earlier stage in the thesis where the WAXD obtained results were discussed.

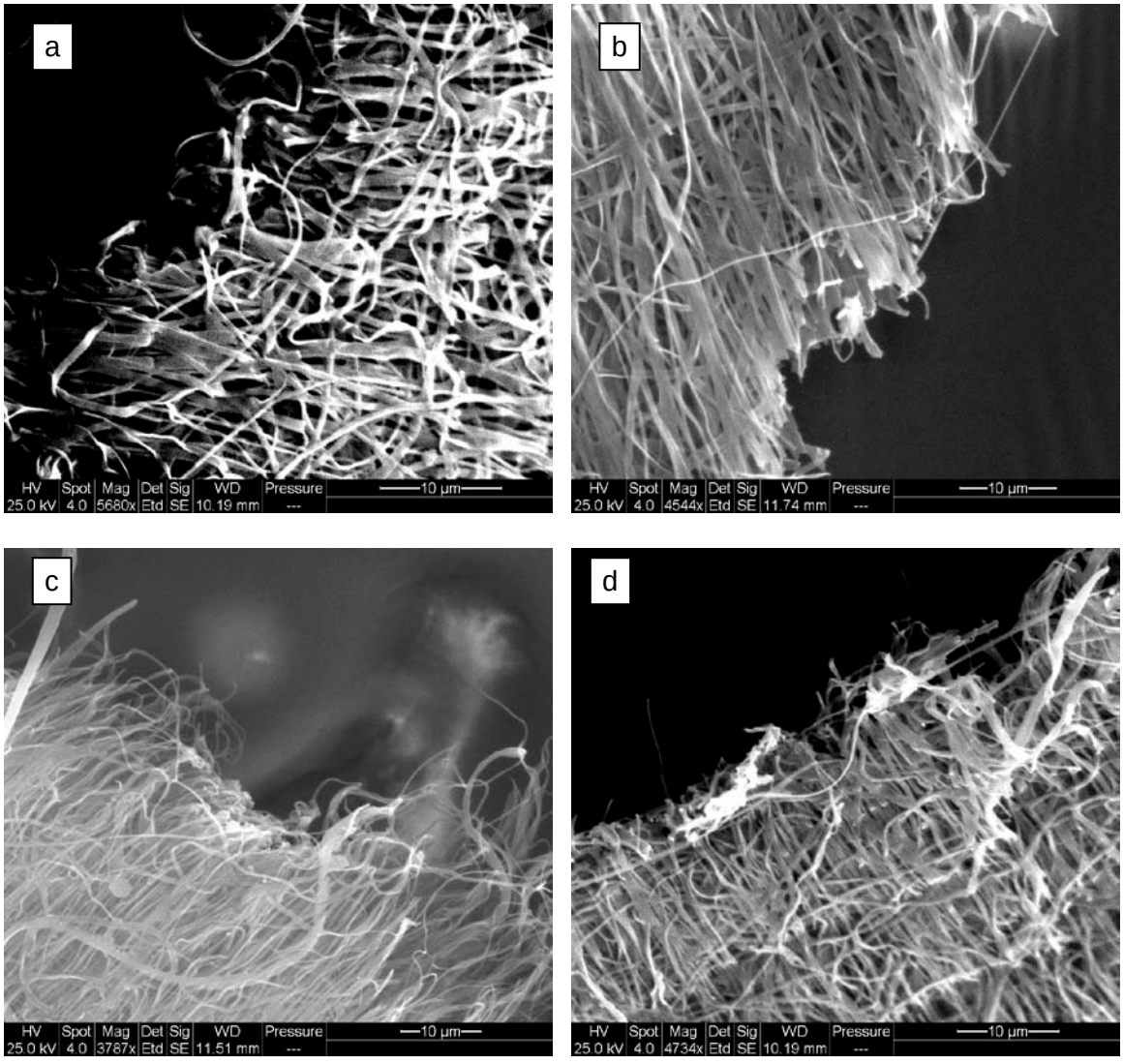

Figure 4.18 SEM micrographs of fiber specimen after being subjected to tensile testing for fibers collected at TUV(s) of (a) 14.2, (b) 17.8, (c) 19.6, and (d) 21.4 m/s.

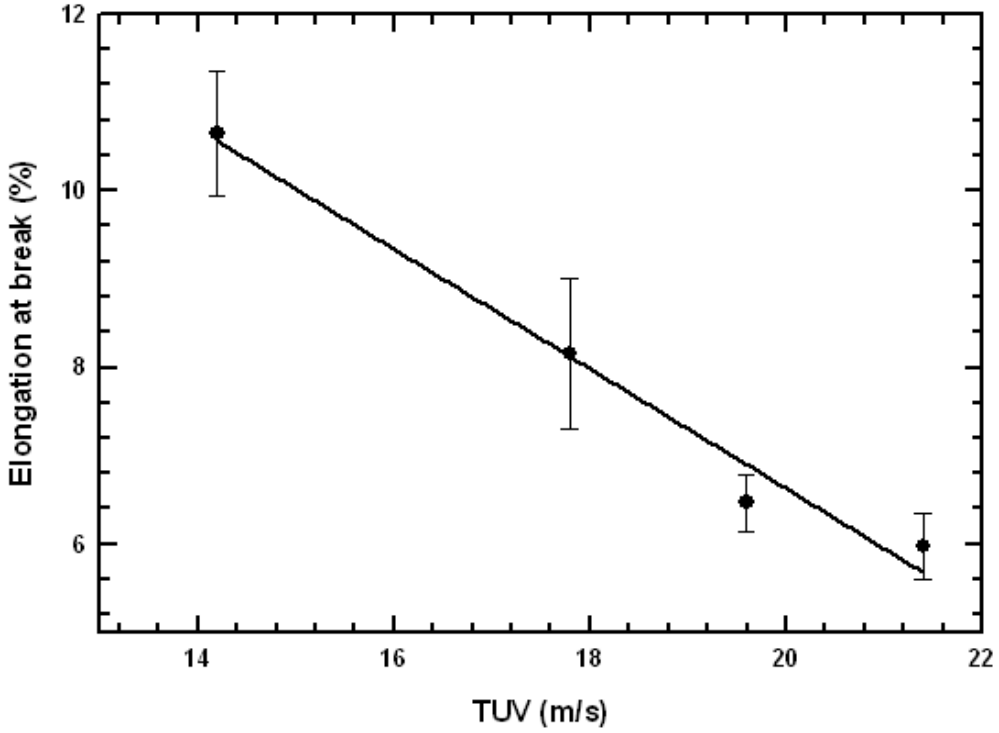

Figure 4.19 Plot of elongation at break vs. TUV.

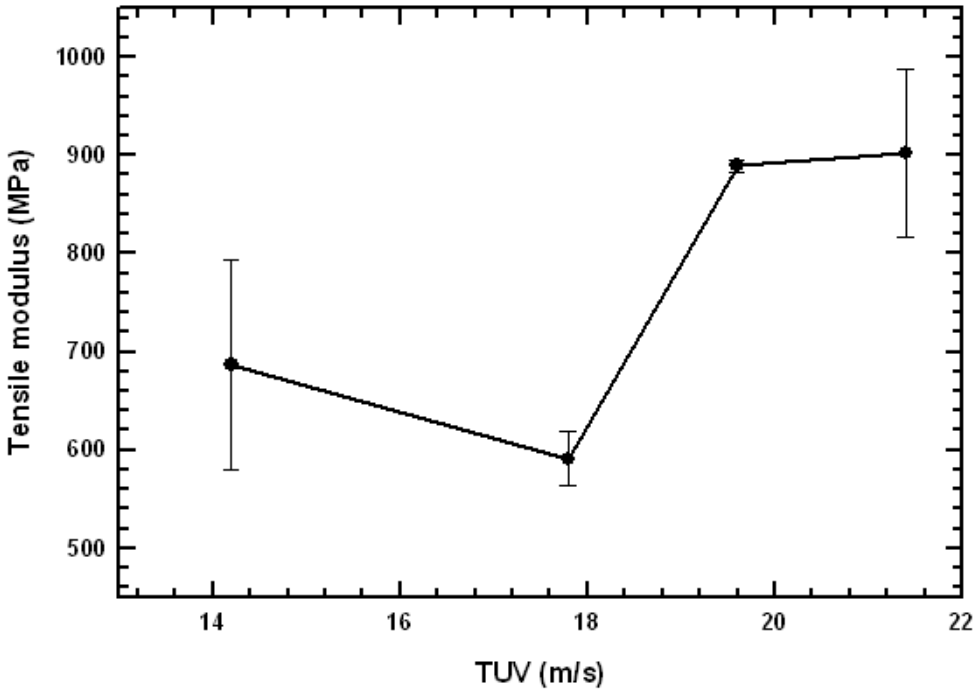

Figure 4.20 Plot of tensile modulus vs. TUV.

Based on the X-ray analysis of crystals shown in Table 4.2, the percentage of α-form crystals in fact increase by 5% in the fibers. These forms of crystals have, as previously mentioned, higher tensile modulus properties compared to the γ-form crystals. Therefore, these characteristics explain the increase of the tensile modulus of the fibers. Figure 4.21 shows the plot of the tensile strength vs. TUV. Whereas the elongation at break decreases, it is obvious from Figure 4.21 that the tensile strength increases by 18.6%. The increase in the molecular orientation and decrease in fiber diameter due to the TUV are also affecting the tensile strength by significantly increasing its value. That shows that the TUV has an effect on the elongation at break, tensile modulus and strength.

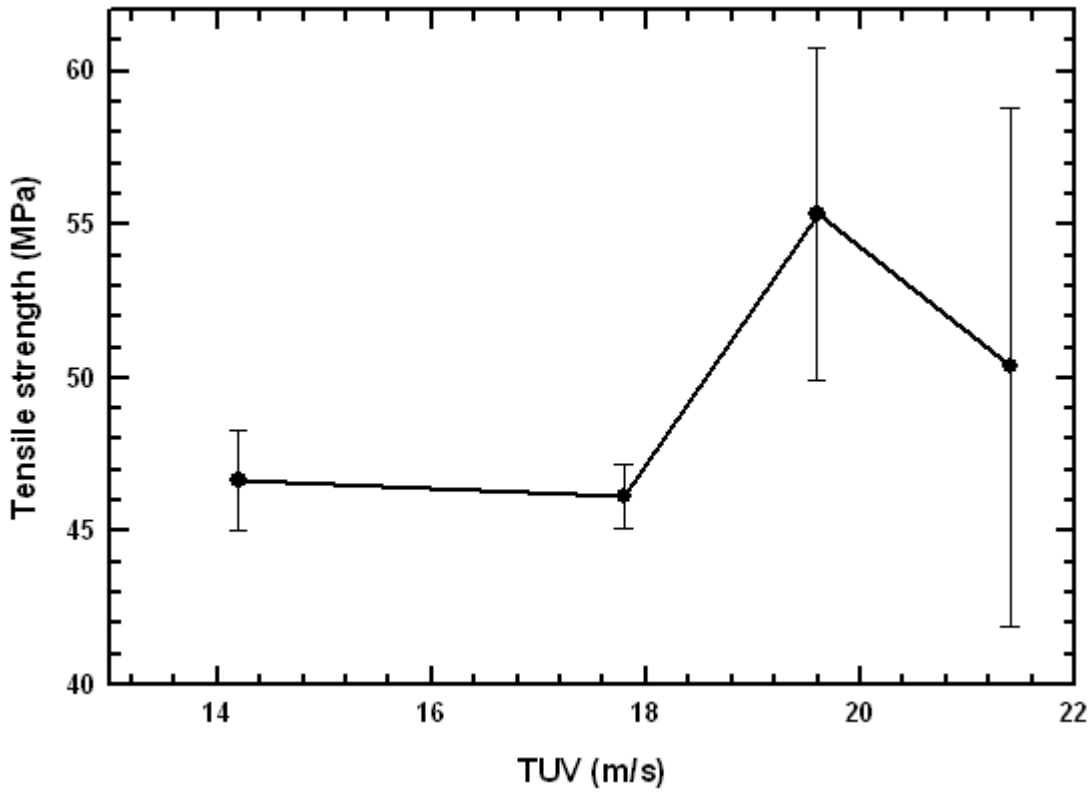

Figure 4.21 Plot of tensile strength vs. TUV.

Table 4.3 summarizes the obtained values for the elongation at break and tensile strength and modulus.

Table 4.3 Variation of tensile modulus, tensile strength, and elongation at break with TUV.

TUV (m/s)	Tensile modulus (MPa)	Tensile strength (MPa)	Elongation at break (%)
14.2	686.1	46.7	10.6
17.8	590.5	46.1	8.2
19.6	889.2	55.3	6.5
21.4	902.9	50.4	6.0

4.4. DSC analysis

The fibers were tested using a DSC machine in order to determine their T_m. Figure 4.22 shows representative curves of the heat flow vs. temperature for the fibers compared to the one of a compression molded sample from bulk.

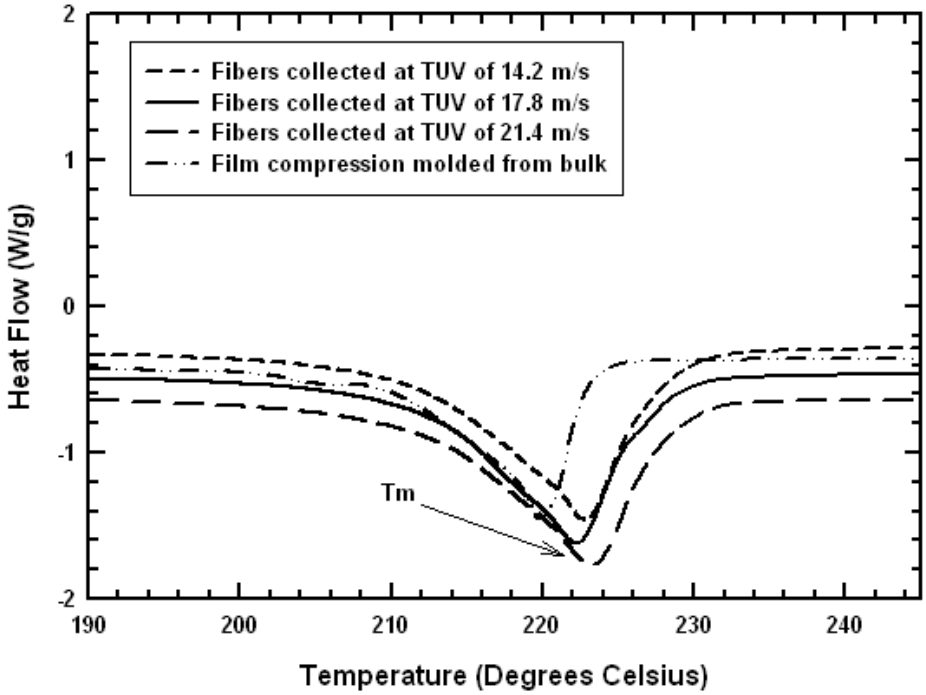

Figure 4.22 Representative curves of heat flow vs. temperature.

It is obvious that the heat of fusion exhibits a peak at around 220. Therefore, it is concluded that the T_m of the fibers occurs at roughly 220 ˚C where the crystals, present in the fibers, melt. Thus, the T_m is not affected by the current fiber diameter, the molecular confinement, or molecular orientation as shown elsewhere [8, 16]. Furthermore, researchers found that 200 nm diameter electrospun nylon 6 fibers melt at around 220˚C which is the same melting temperature for bulk nylon 6 [16, 27]. For clarity, Figure 4.23 shows representative curves of the shifted heat flow vs. temperature for the fibers compared to the one of a compression molded sample from bulk.

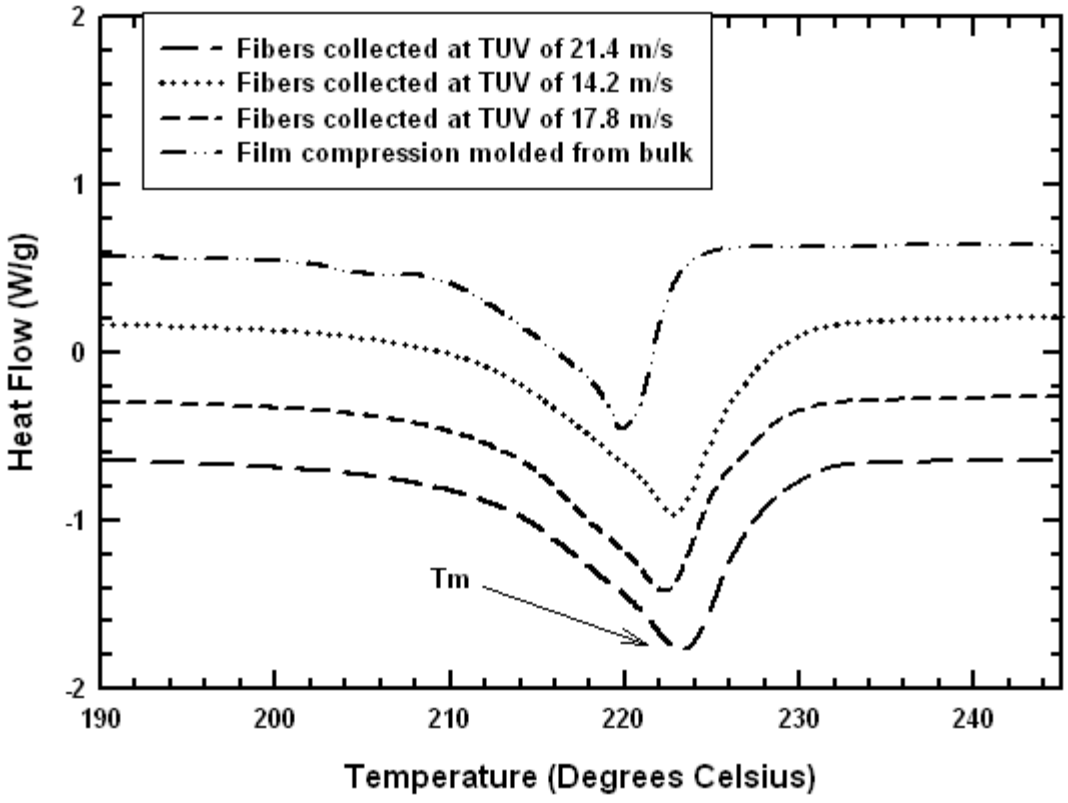

Figure 4.23 Representative curves of shifted heat flow vs. temperature.

4.5. DMA analysis

The T_g of the electrospun nylon 6 fibers was determined by conducting DMA testing on the fibers. Figures 4.24 and 4.25 respectively show representative curves of the tangent delta and storage modulus of the fibers vs. temperature. From Figure 4.24, it is obvious that the β- transition peaks appear for the fibers electrospun at TUV(s) of 17.8 (25 ˚C) and 21.4 m/s (0 ˚C). This transition is due to the presence of moisture in the sample [24, 42, 43]. In case of the fibers electrospun at a TUV of 14.2 m/s, the peak is absent which proves that the fibers do not contain moisture. It could then be concluded that with increasing TUV, the percentage of moisture increases in the fibers.

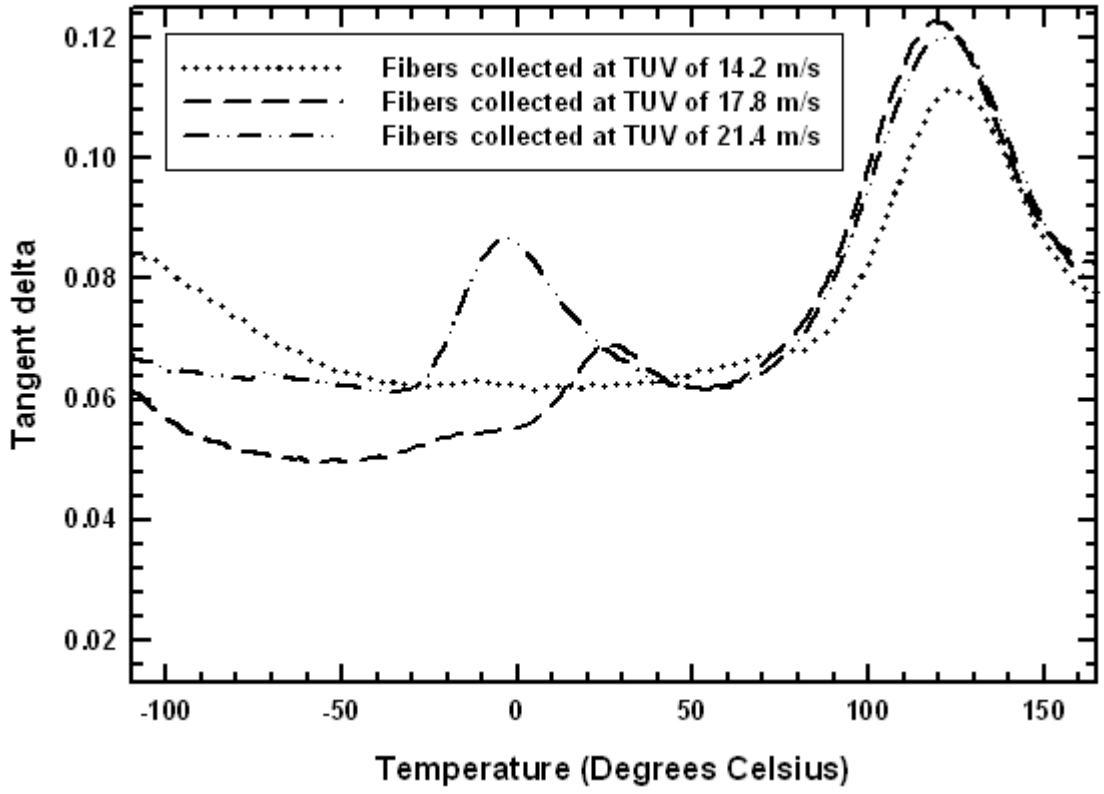

Figure 4.24 Representative curves of tangent delta vs. temperature.

Also, the α-transition peaks appear for the fibers electrospun at TUV(s) of 14.2 (120˚C), 17.8 (120 ˚C) and 21.4 m/s (120 ˚C). The α-transition peak is considered the T_g of the tested sample. It is clear from Figure 4.24 that the T_g remains constant with increasing the TUV.

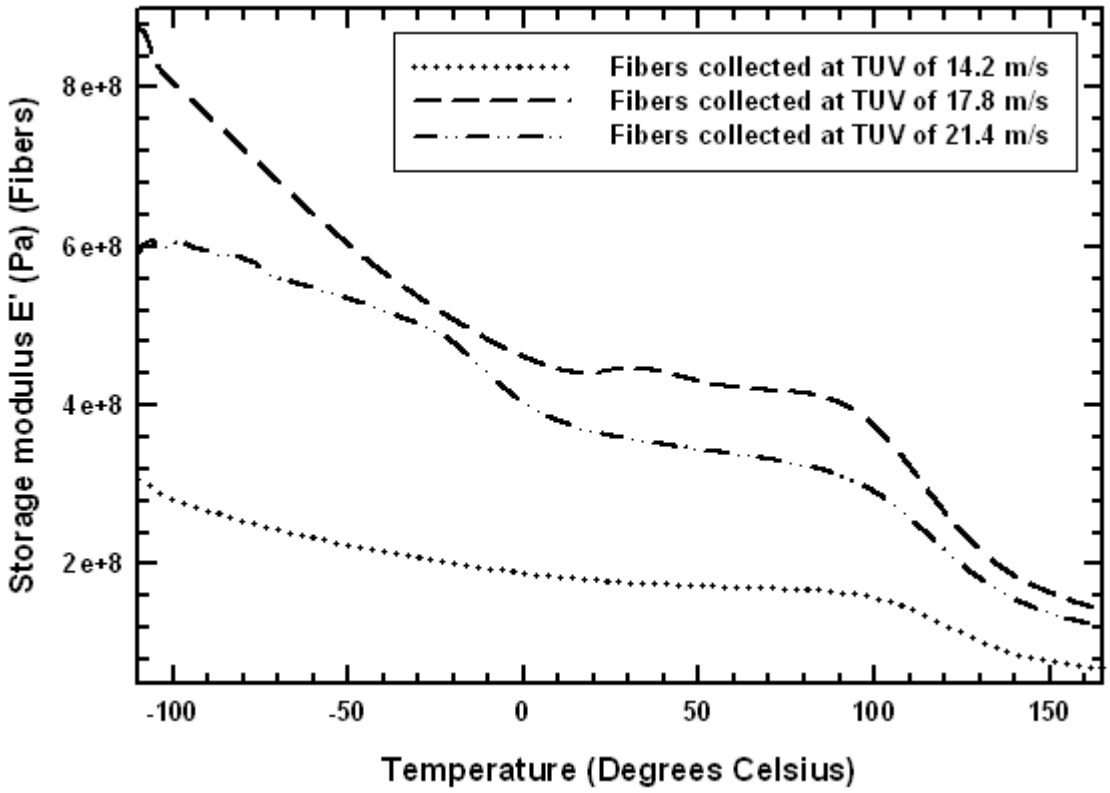

Figure 4.25 Representative curves of storage modulus E' vs. temperature.

CHAPTER V

CONCLUSIONS

5.1. Conclusions

The variation of tensile and thermal properties with TUV was studied for aligned electrospun nylon 6 fibers. The average fiber diameter gradually decreased with increasing the TUV. At the same time, there was a significant increase in the tensile strength and modulus with a significant decrease in the elongation at break when the TUV increased. From WAXD analysis, it was determined that the molecular and crystalline orientations slightly increased with increasing the TUV while the percentage of crystallinity gradually increased. At the same time, the percentage of α-form crystals gradually increased while the percentage of γ-form crystals slightly increased. However, the T_m and T_g of the aligned fibers remained constant with increase of TUV.

5.2. Future work

The importance of adhesion, electrical conductivity, tensile and thermal properties have been a point of focus for the nanotechnology field in order to better understand the behavior of nanometer devices. Therefore, it is significant to study the variation of the adhesion and electrical conductivity with the TUV for electrospun fibers between 40 and 1000 nm. Hence, in future research, we will investigate these phenomena using atomic

force microscopy (AFM), WAXD, and SEM. Annealing the fibers has been shown to be effective in changing the crystalline morphology. Thus, the phenomena mentioned above will be investigated prior to and after annealing the fibers. It has been shown that the electrical conductivity increases with decreasing the average nanotube diameter [157]. Furthermore, it has been determined that the average fiber diameter decreases with TUV. Consequently, it is expected that the electrical conductivity of the electrospun fibers will increase with increasing the TUV. From the other side, the variation of tensile properties with the TUV will be investigated using MTS NanoBionix where representative curves of force per unit weight vs. strain will be shown.

REFERENCES

1. Dosunmu O, Chase G, Kataphinan W, Reneker D. *Nanotechnology* 2006;17:1123

2. Ji Y, Ge S, Li B, Sokolov J, Rafailovich M. *Langmuir* 2006; 22:1321

3. Zussman E, Burman M, Yarin A, Khalfin R, Cohen Y. *J. Polym. Sci.: Part B: Polym. Phys.* 2006; 44:1482

4. Han T,Yarin A, Reneker D. *Polymer* 2008,49,1651-1658

5. Arinstein A, Burman M, Gendelman O, Zussman E. *Nature Nanotechnology* 2007; 2: 59

6. Theron A, Zussman E, Yarin A. *Nano-technology* 2001,12,384-390

7. Huang Z, Zhang Y, Kotaki M, Ramakrishna S. *Comp. Sci. and Tech.* 2003; 63:2223

8. Wong SC, Baji A, Leng S. *Polymer* 2008; 49:4713

9. Inai R, Kotaki M, Ramakrishna S. *Nanotechnology* 2005;16;208

10. Reneker D, Chun I. *Nanotechnology* 1996;7:216

11. Doshi J, Reneker D. *Electrostatics* 1995; 35:151

12. Frenot A, Chronakis I. *Current Opinion in Colloid and Interface Science* 2003; 8: 64

13. Gianchandani J, Spruiell JE, Clark ES. *J. Appl. Polym. Sci.* 1982; 27: 3527

14. Bankar VG, Spruiell JE, White JL. *J. Appl. Polym. Sci.* 1977; 21: 2341

15. Dersch R, Liu T, Schaper AK, Greiner A, Wendorff JH. *J. Polym. Sci. Part A: Polym. Chem.* 2003; 41: 545

16. Jose MV, Steinert BW, Thomas V, Dean DR, Abdalla MA, Price G, Janowski GM. *Polymer* 2007; 48: 1096

17. Murase S, Kashima M, Kudo K, Hirami M. *Macromel. Chem. Phys.* 1997; 198: 561

18. Kongkhlang T, Tashiro K, Kotaki M, Chirachanchai S. *J. Am. Chem. Soc.* 2008; 130: 46, 15460

19. Bolton, E.K.; Ind. Eng. Chem., 1942, 34, 53

20. Schaaf, S. *Faserforsch Textiltech*, 1959; 10: 328

21. Mark H, Whitby GS Eds. Collected Papers of W.H Carothers, Interscience Publishers, Inc., New York, 1940

22. Flory P J. U.S. Patent, 1941; 2,244,192

23. Wichterle O, Tomka J, Sebenda J. *Collect. Czech. Chem. Commun.* 1964; 29: 610

24. Puffr R, Kubanek V. *Lactam-Based Polyamides*, Vol. 1, CRC Press, Boston, 1991; 30

25. Starkweather, HW Jr, Whitney, JF, Johnson DR. J. *Polym. Sci.* Part A 1963; 715:1

26. Fornes TD, Paul DR. *Polymer* 2003; 44: 3945

27. Liu Y, Cui L, Guan F, Gao Y, Hedin NE, Zhu L, Fong H. *Macromolecules* 2007; 40: 6283

28. Starkweather HW Jr, unpublished data

29. Inone M. *J. Polym. Sci.* 1961; 55: 753

30. Brill RJ. *Prakt. Chem*. 1942; 161: 49

31. Slichter WP. *J. Polym. Sci.* 1958; 35: 77

32. Slichter WP. *J. Appl. Phys.* 1955; 26: 1099

33. Willbourn AH. *Trans. Faraday Soc.* 1958; 54: 717

34. Saotome K, Komoto H. *J. Polym. Sci.* Part A-1, *Polym. Chem.* 1966; 4: 1475

35. Woodward AE, Sauer JA. *Fortschr. Hochpolym. Forsch.* 1958; 1: 114

36. Kohan MI. Ed., *Nylon Plastics,* Interscience, New York, 1973

37. Sauer JA, Lim T. *J Macromol. Sci. Phys.* 1977; B13: 419

38. Kawaguchi T. *J Appl. Polym. Sci.* 1959; 2: 56

39. Illers KH. *Polymer* 1977; 18: 551

40. Bershtein VA, Kalinina NA, Stepanov VA. *Mech. Polim.* 1972; 919

41. Starkweather HW Jr. *Water in Polymers, ACS Symp. Ser.* 1980; 127: 433

42. Kettle GJ. *Polymer* 1977; 18: 742

43. Malkin AYa, Dukor AA, Uchastkin VI, Vittadini G. *Vysokomol. Soedin. Ser.* A 1980; 22: 910

44. Birkinshaw C, Buggy M, Daly S. *Polym. Commun.* 1987; 28: 286

45. Mandelkern L. *Crystallization of Polymers,* McGraw-Hill, New York, 1964

46. Ohta T. *Polym. Eng. Sci.* 1983; 23: 679

47. Gogalewski S. *Polymer* 1977; 18: 63

48. Manley TR, Martin CG. *Polymer* 1973; 14: 632

49. Starkweather HW Jr. *J Polym. Sci. Polym. Phys. Ed.* 1981; 19: 1211

50. Geil PH. *Polymer Single Crystals,* Interscience, New York, 1963

51. Hendus H, Illers KH, Simak P. *Kolloid Z.Z. Polymere* 1969; 235: 1244

52. Kogan MI. Ed. *Nylon Plastics,* Interscience, New York, 1973

53. Wunderlick B, Liberti F. *Bull. Amer. Phys. Soc.* 1966; 11: 248

54. Roldan LG, Kaufman HS. *J Polym. Sci. Part B1* 1963; 603

55. Frank O, Wendorff JH. *Colloid, Polym. Sci.* 1981; 259: 1047

56. Peterlin A. *Int. J. Fracture* 1975; 11: 761

57. Weibusch K, Richter R. *J Mater. Sci.* 1986; 21: 3302

58. Buchanan DR, Walters JP. *Text Res. J.* 1977; 47: 398

59. Kettle GJ. *Polymer* 1977; 18: 742

60. Starkweather HW Jr. *Water in Polymers, ACS Symp. Ser.* 1980; 127: 433

61. Jinen E. *J. Mater. Sci.* 1987; 22: 1956

62. Miyake A. *J Polym. Sci.* 1960; 44: 223

63. Heuvel HM, Huisman R. *J Polym. Sci. Polym. Phys. Ed.* 1981; 19: 121

64. Heuvel MM, Huisman R. *J Appl. Polym. Sci.* 1981; 26: 713

65. Bankar SV, Spuriell JE, White LJL. *J Appl. Polym. Sci.* 1977; 21: 2341

66. Tagaki Y, Hattori H, Milkushima Y. *Chem. High Polym.* 1964; 21: 398

67. Sakurada I, Kaji K. *J. Polym. Sci. Polym. Symp.* 1970; 31: 57

68. Manley TR, Martin CG. *Polymer* 1973; 14: 632

69. Kinloch AJ, Young RJ. *Fracture Behaviour of Polymers,* Applied Science Publishers, London 1983; 46

70. Ohta T. *Polym. Eng. Sci.* 1983; 23: 679

71. Prevorsek DC, Garget PJ, Sharma RK, Reimschuessel AC. *J Macromol. Sci.* 1973; B8: 127

72. Peterlin A. *Makromol. Chem.* 1972; 8: 227

73. Gilman TH, Resetarits MR, Crist B Jr. *Polym. Eng. Sci.* 1978; 18: 477

74. Misra A, Dutta B, Prasad VK. *J.* Appl. Polym. *Sci.* 1986; 31: 441

75. Chuah HH, Porter RS. *Polymer* 1986; 27: 241

76. Manley TR, Martin CG. *Polymer* 1973; 14: 632

77. Gogolewski G, Pennings AJ. *Polymer* 1985; 26: 1394

78. Miyasaka K, Isomoto T, Koganeya k, Uehara K, Ishikawa K, Ogata N. *J Polym. Sci. Polym. Phys. Ed.* 1980; 18: 1047

79. Zachariades AE, Porter RS. *J. Polym. Sci. Polym. Lett. Ed.* 1979; 17: 277

80. Kanamoto T, Zachariades AE, Porter RS. *J. Polym. Sci. Polym. Phys. Ed.* 1982; 20: 1485

81. Sakurada I, Kaji D. *J. Polym. Sci. Part C* 1970; 31: 57; *Makromol. Chem. Suppl.* 1975; 1: 599

82. Manley TR, Martin CG, *Polymer* 1973; 14: 632

83. Reneker DH, Chun I. *Nanotechnology* 1996; 7: 216

84. Doshi J, Reneker DH. *J. Electrostat.*1995; 35: 151

85. Wong SC, Baji A, Leng SW. *Polymer* 2008; 21: 4713

86. Arinstein A, Burman M, Gendelman O, Zussman E. *Nat. Nanotech.*2007; 2: 59

87. Tan EPS, Ng SY, Lim CT. *Biomaterials* 2005; 26: 1453

88. Zussman E, Burman M, Yarin AL, Khalfin R, Cohen Y. *J. Polym. Sci. Part B: Polym. Phys.* 2006; 44: 1482

89. Lannutti J, Reneker D, Ma T, Tomasko D, Farson D. *Mater. Sci. Eng. (Biomim. Supramol. Sys.)* 2007; 27: 504

90. Dror Y, Salalha W, Khalfin RL, Cohen Y, Yarin AL, Zussman E. *Langmuir* 2003; 19: 7012

91. Salalha W, Dror Y, Khalfin RL, Cohen Y, Yarin AL, Zussman E. *Langmuir* 2004; 20: 9852

92. Li WJ, Laurencin CT, Caterson EJ, Tuan RS, Ko FK. *J. Biomed. Mater. Res.* 2002; 60: 613

93. Fong H. *Polymer* 2004; 45: 2427

94. Tian M, Gao Y, Liu Y. *Polymer* 2007; 48: 2720

95. Kim JS, Reneker DH. *Polym. Compos.* 1999; 20: 124

96. Zhang M, Atkinson KR, Baughman RH. *Science* 2004; 306:1358

97. Formhals, A. *US patent no. 1975504* 1934

98. Reneker DH, Yarin AL, Fong H, Sureeporn K. *J. Appl. Phys.* 2000; 87: 4531

99. Shin YM, Hohman MM, Brenner MP, Rutledge GC. *Polymer* 2001; 42: 9955

100. Shin YM, Hohman MM, Brenner MP, Rutledge GC. *Appl. Phys. Lett.* 2001; 78: 1149

101. Fang X, Reneker DH. *J. Macromol. Sci.-Phys.* 1997; B36: 169

102. Taylor GI. *Proc. R. Soc. London*, Ser. A 313, 453 (1969)

103. Taylor GI. Electrically Driven Jets. *Proc. R. Soc. London*, Ser. A 291, 145 (1966)

104. Hohman MM, Shin M, Rutledge G. *Phys. Fluids.* 2001; 13:2201

105. Fridrikh SV, Yu JH, Brenner MP, Rutledge GC. *Phys. Rev. Lett*. 2003; 90: 1

106. Eda G, Shivkumar S. *J. Mater. Sci.* 2006; 41: 5704

107. Liu H, Hsieh YL. *J. Polym. Sci. Part B: Polym. Phys.* 2002; 40: 2119

108. Kim HS, Kim K, Jin HJ, Chin IJ. *Macromol. Symp.* 2005; 224: 145

109. Sundaray B, Subramanian V, Natarajan TS, Xiang RZ, Chang CC, Fann WS. *Appl. Phys. Lett.* 2004; 84: 1222

110. Katta P, Alessandro M, Ramsier RD, Chase GG. *Nano. Lett.* 2004; 4: 2215

111. Theron A, Zussman E, Yarin AL. *Nanotechnology* 2001; 12: 384

112. Fennessey SF, Farris RJ. *Polymer* 2008; 45: 4217

113. Sill TJ, Recum HAV. *Biomaterials* 2008; 29: 1989

114. Huang ZM, Zhang YZ, Kotaki M, Ramakrishna S. *Comp. Sci. Technol.* 2003; 63: 2223

115. Mathew G, Hong JP, Rhee JM, Lee HS, Nah C. *Polym.Test.* 2005; 24: 712

116. Xu CY, Inai R, Kotaki M, Ramakrishna S. *Biomaterials* 2004; 25: 877

117. Dersch R, Liu T, Schaper Ak. *J. Polym. Sci.: part A: Polym. Chem.* 2003; 41: 545

118. Teo WE, Ramakrishna S. *Nanotechnology* 2005; 16: 1878

119. Kim GH, Kim WD. *Appl. Phys. Lett.* 2006; 88: 233101

120. Teo WE, Ramakrishna S. *Nanotechnology* 2006; 17: 89

121. Konkhlang T, Tashiro K, Kotaki M, Chirachanchai S. *J. Am. Chem. Soc.* 2008; *130*, 15460

122. Lim CT, Tan EPS, Ng Sy. *Appl. Phys. Lett.* 2008; 92: 141908 .

123. Baji, A, Wong SC, Blackledge TA, Leng, S. *ANTEC Conf Proc* 2008.

124. Zong XH, Kim K, Fang DF, Ran SF, Hsiao BS, Chu B. *Polymer* 2002; 43: 4403

125. Brazinsky I, Williams AG, LaNieve HL. *Eng. Sci.* 1975; 15: 834

126. Wang H, Shao H, Hu X. *J. Appl. Polym. Sci.* 2006; 101: 961

127. White JL, Hancock TA. *J. Appl. Polym. Sci.* 1981; 21: 3157

128. Greiner A, Wendorff JH. *Angew. Chem.-Int. Edit.* 2007; 46: 5670

129. Lee KH, Kim HY, La YM, Lee DR, Sung NH. *J. Polym. Sci. Part B: Polym. Phys.* 2002; 40: 2259

130. Reneker DH, Kataphinan W, Theron A, Zussman E, Yarin AL. *Polymer* 2002; 43: 6785

131. Prilutsky S, Zussman E, Cohen Y. *Nanotechnology* 2008; 19: 165603(9pp)

132. Curgul S, Vliet KJV, Rutledge GC. *Macromolecules* 2007; 40: 8483

133. Ngai KL. *J. Polym. Sci. Part B Polym. Phys.* 2006; 44: 2980

134. Ngai KL. *Eur. Phys. J. E.* 2002; 8: 225–235

135. Kim WH, Lee KH, Khil MS, Ho SY, Kim HY. *Polym.* 2004; 5: 122

136. Yee WA, Nguyen AG, Lee PS, Kotaki M, Liu Y, Tan BT. *Polymer* 2008; 49:4196

137. Shields KJ, Beckman MJ, Bowlin GL. *Tiss. Eng.* 2004; 10: 1510

138. Lu JW, Zhang ZP, Ren XZ, Chen YZ, Yu J, Guo ZX. *Macromolecules* 2008; 41: 3762

139. Wu XF, Dzenis YA. *J. Appl. Phys.* 2007; 102: 044306 .

140. Thomas V, Jose MV, Chowshury S, Sullivan JF, Dean DR, Vohra YK. *J. Biomater. Sci Polym. Ed.* 2006; 17: 969

141. Huang C, Chen S, Reneker DH. Lai CL, Hou HQ. *Adv. Mater.* 2006; 18:668

142. Chen F, Peng X, Li T, Chen S, Wu XF, Reneker DH, Hou H. *J. Phys. D: Appl. Phys.* 2008; 41:025308

143. Wang YZ, Blasioli DJ, Kim HJ, Kim HS, Kaplan DL. *Biomaterials* 2006; 27: 4434

144. Moroni L, Licht R, de Boer J, de Wijn JR, van Blitterswijk CA. *Biomaterials* 2006; 27: 4911

145. Yoshimoto H, Shin YM, Terai H, Vacanti JP. *Biomaterials* 2003; 24: 2077

146. Goldberg M, Langer R, Jia XQ. *J. Biomat. Sci.-Polym. Ed*. 2007; 18: 241

147. Baji A, Wong SC, Srivatsan TS, Njus GO, Matur G. *Mater. Manufac. Proc*. 2006; 21: 211

148. Bergshoef MM, Vancso GJ. *Adv. Mater.*1999; 11: 1362

149. Norris ID, Shaker MM, Ko FK, MacDiarmid AG. *Synth. Met.* 2000; 114: 109

150. MacDiarmid AG, Jones WE, Norris ID, Gao J, Johnson AT, Pinto NJ, Hone J, Han B, Ko FK, Okuzaki H, Llaguno M. *Synth. Met.* 2001; 19: 27

151. Yoon K, Hsiao BS, Chu B. *J. Mater. Chem.* 2008; 18: 5326

152. Heikkila P, Taipale A, Lehtimaki M, Harlin A. *Polym. Eng. Sci.* 2008; 48: 1168

153. Barhate RS, Loon CK, Ramakrishna S. *J. Membrane. Sci.* 2006; 283: 209

154. Chen S, Hu P, Greiner A, Cheng C, Cheng H, Chen F, Hou H. *Nanotechnology* 2008; 19: 15604

155. Rahman N, Kawai T, Matsuba G, Nishida K, Kanaya T, Watanabe H, Okamoto H, Kato M, Usuki A, Matsuda M, Nakajima K, Honma N. *Macromolecules* 2009; 42: 4739

156. Samuel RJ. Structured Polymer Properties. New York, Whiley-Interscience. 1974

157. Cuenot S, Demoustier-Champagne S, Nysten B. *Physical Review Letters* 2000; 85: 1690